UCRL-TR-218833

LAWRENCE LIVERMORE NATIONAL LABORATORY

FY05 LDRDFinal Report Chemical Dynamics at Interfaces

E. Schwegler, T. Ogitsu, S. Bonev, A. Correa, B. Militzer, G. Galli

February 13, 2006

Disclaimer

This document was prepared as an account of work sponsored by an agency of the United States Government. Neither the United States Government nor the University of California nor any of their employees, makes any warranty, express or implied, or assumes any legal liability or responsibility for the accuracy, completeness, or usefulness of any information, apparatus, product, or process disclosed, or represents that its use would not infringe privately owned rights. Reference herein to any specific commercial product, process, or service by trade name, trademark, manufacturer, or otherwise, does not necessarily constitute or imply its endorsement, recommendation, or favoring by the United States Government or the University of California. The views and opinions of authors expressed herein do not necessarily state or reflect those of the United States Government or the University of California, and shall not be used for advertising or product endorsement purposes.

Auspices Statement

This work was performed under the auspices of the U. S. Department of Energy (DOE) by the University of California, Lawrence Livermore National Laboratory (LLNL) under Contract No. W-7405-Eng-48. The project (03-ERD-001) was funded by the Laboratory Directed Research and Development Program at LLNL.

FY05 LDRD Final Report
Chemical Dynamics at Interfaces
LDRD Project Tracking Code: 03-ERD-001

Eric Schwegler (PI), Tadashi Ogitsu, Stanimir Bonev, Alfredo Correa, Burkhard Militzer, and Giulia Galli

Abstract
This project has been focused on the development and application of *ab initio* simulation methods to study at the microscopic level a variety of complex interfacial systems under extreme conditions. By building on our existing expertise in first principles molecular dynamics, we have developed new techniques for the calculation of melting lines entirely from first principles (two-phase simulation methods). The simulation methods developed in this project have been applied to a set of low-Z materials that are relevant to potential NIF early light experiments.

Introduction/Background
The presence of an interface is central to many areas of science ranging from the study of physical properties such as melting and structural phase transitions, to chemical properties such as catalysis and corrosion resistance. In fact, many chemical processes depend on an interface for both the location and the driving force for reactions that would not normally occur in a bulk-phase environment. Despite their importance and significance, until recently, very little has been known about interfacial processes at a microscopic level. However, new experimental measurements are beginning to appear where interactions near an interface are selectively probed. In addition to these important experimental developments, molecular simulations may play a central role in increasing our understanding of interfacial systems. Predictive simulations can be used to complement experimental measurements, and also to investigate systems for which measurements do not yet exist. For example, liquid-solid coexistence simulations were used to both resolve the differences between existing static and shock compressed measurements of iron melting, and to extend the melting line to pressures that have not yet been measure[1].

While simulations have the potential of adding a great deal to our understanding of interfacial systems at a molecular level, they are quite challenging from a computational point of view. As compared to independent (single-phase) simulations, interfacial systems under extreme conditions introduce extra levels of complexity:

- There are few, if any, reliable empirical parameters for complex molecular systems that involve multiple chemical species and/or a large range of thermodynamics conditions.
- Interfacial systems often involve chemical reactions that do not occur in the bulk phases. Therefore, realistic modeling of an interface often necessitates

the use of a method that quantitatively describes bond making and breaking processes.
- The requirements on system sizes are more severe for models of interfaces than for models of single-phase systems, and thus the use of sophisticated simulation models are more challenging from a computational viewpoint.

In order to address these issues, our approach was to use methods based on first-principles electronic structure theory, which allowed us to examine the behavior of interfacial systems under thermodynamic conditions relevant to static and dynamic high-pressure experiments. For these types of systems, the use of first principles methods proved to be crucial because it provided a number of key benefits that include:

- A reliable description of complex molecular systems, for which suitable empirical parameters are not available.
- The ability to examine thermodynamic conditions where there are little or no experimental data available (extreme temperatures and pressures) and for which predictive techniques are needed.
- A quantitative description of complex reactions that might take place, e.g. in shock compressed materials. The breaking and making of chemical bonds needs to be described with quantum mechanical accuracy.
- Additional detailed information that can be obtained from knowledge of the electronic structure properties.

The primary focus of this project was on solid-liquid interfacial systems, and in particular, on efficient methods for determining melting curves of a material as a function of pressure. There exist a variety of different approaches for mapping out phase boundaries. At zero-temperature, the transition pressure is simply defined by the crossing point of enthalpy curves; while, at finite temperatures, one has to calculate the free energy*, i.e.*, take into account entropic contributions. The former requires only the static total energy curve as a function of volume, while the latter requires an ensemble average over configuration space.

The simplest way to calculate the Helmholtz free energy is within the harmonic approximation (or quasi-harmonic approximation)[2]. We have applied this method to unravel the phase diagram of a variety of different materials. For example, by combining static density functional theory total energy calculations with the harmonic approximation, we determined the complex phase diagram of CO_2 where indeed one of the phases, *cmca*, was shown to be entropy driven due to a soft mode in the *cmca* structure[3].

However, there are many cases where the anharmonicity of a material becomes large, and one has to go beyond the harmonic approximation. One approach for achieving this is to use direct molecular dynamics simulations combined with thermodynamic integration and potential switching schemes[4]. Although the general method is conceptually well established, the main difficulty lies in the demanding computational requirements; one has to perform numerous molecular dynamic

simulations to cover wide ranges of volume and temperature space, and ensure the precise convergence of ensemble averages at each thermodynamic point.

An alternative and computationally simpler way for determining solid-liquid phase boundaries has been developed in the context of classical molecular dynamics simulations[5]. This approach is usually referred to as the two-phase simulation method, in which one simply performs molecular dynamics of a system consisting of two phases in contact with each other. In the typical application of this method, the simulation is prepared by first performing single-phase simulations of a solid and a liquid at a given temperature and pressure. Once equilibration is achieved, the two phases are merged into a single simulation cell and each phase is independently heated under constant volume conditions to reduce the strain at the newly formed interface. A molecular dynamics simulation of the entire system is then performed in the *N-P-T* ensemble (constant number of particles, pressure and temperature respectively). As the simulation progresses, the interfacial region can be monitored and depending on the relative stability of the liquid and the solid, eventually one of the phases will dominate the entire volume available in the simulation. By repeating this process for different temperatures at a fixed pressure, the melting temperature of the material can be effectively bracketed by direct simulation of the melting or solidification process. In practice, this is equivalent to explicit computation and matching of the free energies of the competing phases, but at a much-reduced computational cost.

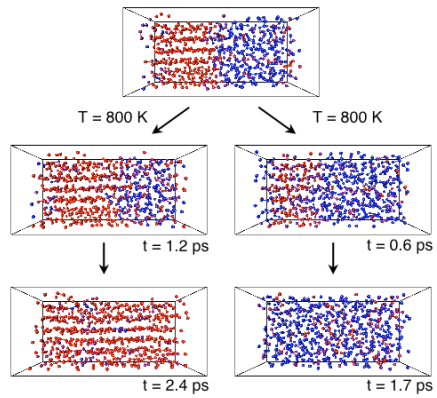

Figure 1. Snapshots from a two-phase simulation of hydrogen at P = 130 GPa and temperatures below and above the melting temperature. The color is determined by the local order around each hydrogen molecule, red corresponds to an hcp structure and blue to a liquid.

It is important to point out that the interfacial region in this approach is crucial to the success of the method. In particular, the presence of the solid-liquid interface avoids the problems associated with superheating or cooling, which occurs in single-phase heat-until-it-melts approaches[6].

In this project, we succeeded in applying the two-phase method, for the first time, with first-principles molecular dynamics to determine the melting line of lithium hydride. We have also recently used this approach to determine the solid-liquid phase boundary in hydrogen, carbon and water.

Research Activities

In the following sections, we briefly describe the main systems that have been examined in this project: lithium hydride, hydrogen, water and carbon. Additional detailed information can be found in the attached papers.

Lithium Hydride:

We have computed the melting line of lithium hydride up to 200 GPa using the two-phase simulation technique coupled with first-principle molecular dynamics. Our predicted melting temperature at high pressures varies slowly with compression, ranging from 2000 to 2450 K at 50-200 GPa pressures. The compressed fluid close to the melting line retains the ionic character of the low pressure molten state, while at higher temperature dynamical hydrogen clustering processes are observed, which are accompanied by changes in the electronic structure.

Hydrogen:

The phase diagram of hydrogen has been extensively studied over the past several decades, with particular interest in the expected molecular dissociation and metallization at high pressure[7]. In 1935, Wigner and Huntington[8] predicted that upon sufficient compression hydrogen forms an alkali-like lattice. Three decades later, Ashcroft[9] proposed that solid metallic hydrogen would be a high-temperature superconductor. The possibility that the metallization transition will lead to a liquid rather than a solid even at low temperature has also been considered[10]. Recent theoretical models suggest that such a state may be a superconductor and a superfluid at the same time[11]. In view of these exciting prospects, establishing the phase diagram of dense hydrogen is clearly of high interest. However, despite a large number of investigations, it still remains unsettled.

We have used the two-phase simulation technique to examine the solid-liquid phase boundary in hydrogen under pressures of 50 to 200 GPa. Our results predict that the melting curve of hydrogen has a negative slope above 90 GPa. Furthermore, we have found strong evidence for the existence of a low-temperature quantum fluid in hydrogen near 400 GPa, a state that would be of extraordinary nature - a zero-temperature liquid metal. In addition to computing the melting curve of hydrogen, we have also determined the physical origin of the maximum, which is related to subtle changes in intermolecular interactions at high pressures, and not to the onset of dissociation in the liquid.

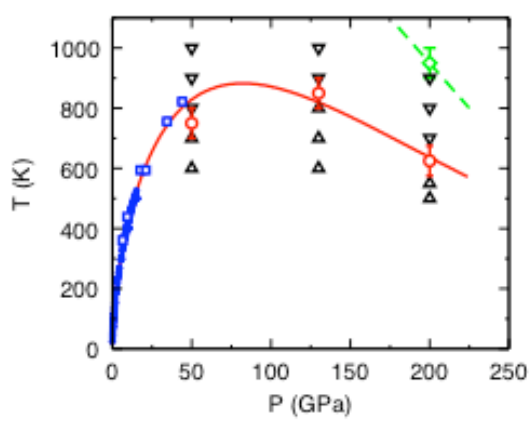

Figure 2. The melting curve of hydrogen. The blue squares are experimental measurements. Triangles indicate two-phase simulations where solidification (up) or melting (down) have been observed.

Water:
The precise determination of the melting curve of water is important for many different problems found in physics, chemistry and planetary sciences. Given the ubiquitous nature of water, it is perhaps surprising to learn that until very recently, various experimental groups have not been able to agree on the melting temperature of water for pressures near 10-20 GPa[12]. With advances in combining techniques such as angle-dispersive synchrotron X-ray diffraction or *in situ* Raman spectroscopy with improved diamond anvil cell technologies, it is now possible to accurately measure the melting temperature of water for pressures up to 35 GPa[13].

Interestingly, a number of experimental measurements have indicated that at even higher pressures, near approximately 35 to 47 GPa, the slope of the melting curve increases rapidly, possibly due to the presence of a triple point. Although this triple point has not been directly characterized by experiment, it has been suggested that it may involve the formation of a superionic phase, dynamically disordered ice-VII, or the location of the ice VII/ice X phase boundary.

Previous first-principles simulations of the melting of ice VII and ice X have favored the interpretation based on a transition to a superionic phase where the oxygen atoms remain fixed in a body-centered-cubic sublattice while the hydrogen atoms diffuse rapidly. Although these simulations are in overall agreement with the existence of a superionic phase in water, they are in poor agreement with each other on the precise location of its melting curve. In particular, different simulations have indicated that at a temperature of 2000 K, superionic water will melt at pressures ranging from 30 GPa[14], to 65 GPa[15], to 75 GPa[16]. These large differences in the melting pressure is somewhat surprising given that nearly identical levels of theory and simulation protocols were used. In addition to possible issues related to finite size effects and simulation timescales, it is likely that a large fraction of this discrepancy comes from the specific computational approach used to determine the phase boundary. In all of the previous calculations, the simulations were based on a single-phase description (either the liquid or the solid) and have proceeded with a "heat-until-it-melts" or a "squeeze-until-it-freezes" strategy for locating the transition between the liquid and the solid phase. As mentioned earlier, the primary

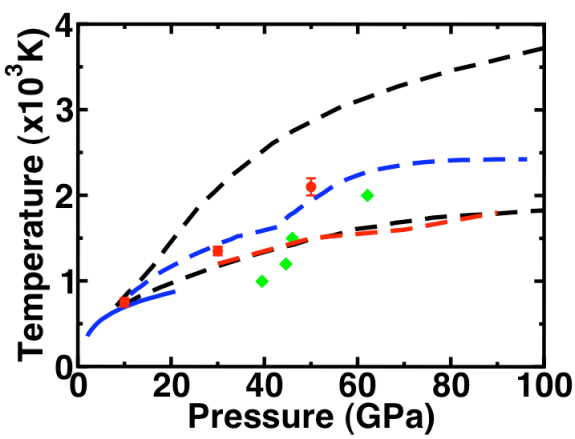

Figure 3. The melting curve of water. The blue solid[13] and dashed lines[17] are experimental measurements. The red circles represent the bracketed melting temperatures obtained by two-phase simulations, and the red dashed line is the onset of significant protonic diffusion. Previous single-phase first-principles estimates of the superionic regime[14] and the melting curve[16] are represented by the dashed black and red curves, respectively.

objection to this approach is that the observed phase transition does not directly correspond to the melting temperature (or pressure), but instead to conditions of thermal instability, which for small system sizes and short simulations timescales can be significantly different from the equilibrium melting point.

In order to examine the possibility of a transition to a superionic phase and to determine the high-pressure melting curve of water, we have performed a series of large-scale (256 molecules) two-phase simulations of water at high-pressures. Our computed melting temperatures at 10, 30 and 50 GPa are 750±50, 1350±50, and 2100±100 K, respectively. These computed melting temperatures are consistent with recent measurements on water obtained with a laser heated diamond anvil cell[17]. In agreement with previous first-principles simulations, we find regions of fast protonic diffusion for temperatures below the melting curve. The transition to this region appears gradual and bears some similarities to a type-II superionic conductor[18].

Carbon:
At high pressure and temperature, the phase diagram of elemental carbon is poorly known. We have examined the diamond and BC8 melting lines and their phase boundary in the solid phase, as obtained from first principles calculations. Maxima are found in both melting lines, with a triple point located at ~850 GPa and ~ 7400 K. Our results show that hot, compressed diamond is a semiconductor, which undergoes metalization upon melting. In contrast, in the stability range of BC8, an insulator to metal transition is likely to occur in the solid phase. Close to the diamond/ and BC8/liquid boundaries, molten carbon is a low-coordinated metal retaining some covalent character in its bonding up to extreme pressures. Our results provide constraints on the carbon equation of state, which is of critical importance for devising models of Neptune, Uranus and white dwarf stars, as well as of extra-solar carbon-rich planets.

Results/Technical Outcome
The primary benefit of this project has been in the development of capabilities at the laboratory for investigating interfacial systems under extreme temperature and pressure conditions. The application of these methods has led to new detailed information on wide range of systems that include hydrogen, lithium hydride, water and carbon. In addition, this work has resulted in a number of high-profile publications in journals such as *Physical Review Letters*, *The Proceedings of the National Academy of Sciences* and *Nature*. In particular, in our article on the melting curve of hydrogen that appeared in the journal *Nature* was highlighted on the cover of that issue. It is also important to note that because the techniques that we have focused on are based on first-principles electronic structure theory, they are completely general and can be applied to a wide range of systems that are relevant to problems in Physics, Chemistry and Biology.

Exit Plan
The computational methods and capabilities developed here have been instrumental in creating a number of new research projects and funding sources for the Quantum Simulations Group. For example, the following ongoing efforts have strongly

benefited from the work carried out in this project: "Quantum Simulations for EOS Prediction and Validation" (Dynamics of Metals), "EOS of Hydrogen and Low-Z Mixtures" (ASC equation-of-state project) and "Melting Calculations" (PDRP). We also note that the first-principles based two-phase methods that we have pioneered are currently being adopted by other groups at the Laboratory to compute the melting of metals as a function of pressure (in direct support of program needs).

Summary

In this project we have examined a variety of low-Z interfacial systems under extreme conditions. The primary focus of this work has been on implementing, for the first time, a two-phase simulation technique for examining solid-liquid phase boundaries within first-principles molecular dynamics. The success of this project has depended heavily on utilizing the unique computational capabilities of the Laboratory. In particular, the application of first-principles molecular dynamics to interfacial systems is currently not feasible without access to a massively parallel computing facility and state-of-the-art simulations codes. Our results have demonstrated that with moderate sized supercells (~500-1000 atoms) and acceptable time scales (~5-10 ps) the melting temperature of a material can be accurately computed as a function of pressure entirely from first-principles. This new capability opens up the possibility of performing systematic studies of melting temperatures with density functional theory for a wide range of materials.

Papers Published

1. Tadashi Ogitsu, Eric Schwegler, François Gygi, and Giulia Galli, "Melting of Lithium Hydride Under Pressure" *Phys. Rev. Lett.* **91**, 175502 (2003) UCRL-JC-153550
2. Burkhard Militzer, François Gygi and Giulia Galli, "Structure and bonding of dense liquid oxygen from first principles simulations" Phys. Rev. Lett. **91**, 265503 (2003) UCRL-JC-152461
3. Stanimir A. Bonev, François Gygi, Tadashi Ogitsu and Giulia Galli, "The high-pressure molecular phases of solid carbon dioxide" Phys. Rev. Lett. **91**, 65501 (2003) UCRL-JC-151202
4. François Gygi, Jean-Luc Fattebert and Eric Schwegler, "Computation of maximally localized Wannier functions using a simultaneous diagonalization algorithm" *Comp. Phys. Comm.* **155**, 1 (2003) UCRL-JC-151591
5. Stanimir A. Bonev, Burkhard Militzer and Giulia Galli, "Ab initio simulations of dense liquid deuterium: Comparison with gas gun shock wave experiments" Phys. Rev. B **69**, 014101 (2004) UCRL-JC-153551
6. Stanimir A. Bonev, Eric Schwegler, Tadashi Ogitsu and Giulia Galli, "A quantum fluid of metallic hydrogen suggested by first-principles calculations" *Nature* **431**, 669 (2004) UCRL-JRNL-206079
7. Alfredo A. Correa, Stanimir A. Bonev and Giulia Galli, "Carbon under extreme conditions: Phase boundaries and electronic properties from first-principles theory" *Proc. Nat. Acad. Sci.* in press (2005) UCRL-JRNL-216286
8. Jung-Fu Lin, Eric Schwegler and Choong-Shik Yoo, "Phase diagram and

physical properties of water at high pressures and temperatures: applications to planetary interiors" in AGU Monograph: Earth's Deep Water Cycle, in press (2006) UCRL-JRNL-215773

References:

[1] A. Laio, S. Bernard, G.L. Chiarotti, S. Scandolo and E. Tosatti, Science **287**, 1027 (2000)

[2] B. B. Karki, R. M. Wentzcovitch, S. de Gironcoli and S. Baroni, Phys. Rev. B **61**, 8793 (2000).

[3] S. A. Bonev, F. Gygi, T. Ogitsu and G. Galli, Phys. Rev. Lett. **91**, 65501 (2003)

[4] M. de Koning, W. Cai, A. Antonelli and S. Yip, Comp. Sci. Eng. **2**, 88 (2000)

[5] J. Mei and J.W. Davenport, Phys. Rev. B **46**, 21 (1992)

[6] A. B. Belonoshko, Amer. Miner. **86**, 193 (2001)

[7] I. F. Silvera, Rev. Mod. Phys. **52**, 393 (1980)

[8] E. Wigner and H. B. Huntington, J. Chem. Phys. **3**, 764 (1935)

[9] N. W. Ashcroft, Phys. Rev. Lett. **21**, 1748 (1968)

[10] N. W. Ashcroft, J. Phys.: Condens. Matter **12**, A129 (2000)

[11] E. Babaev, A. Sudbe and N. W. Ashcroft, Nature **431**, 666 (2004)

[12] J. F. Lin, B. Militzer, V. V. Struzhkin, E. Gregoryanz, R. J. Hemley and H. K. Mao, J. Chem. Phys. **121**, 8423 (2004)

[13] J. F. Lin, E. Gregoryanz, V. V. Struxhkin, M. Somayazulum H. K. Mao and R. J. Hemley, Geophys. Res. Lett. **32**, L11306, 2005.

[14] C. Cavazzoni. G. L. Chiarotti, S. Scandolo, E. Tosatti, M. Bernasconi and M. Parrinello, Science **283**, 44 (1999)

[15] A. F. Goncharov, *et al.* Phys. Rev. Lett. **94**, 125508 (2005)

[16] N. Goldman, *et al.* Phys. Rev. Lett. **94**, 217801 (2005)

[17] B. Schwager, L. Chudinovskikh, A. Gavrilliuk and R. Boehler, J. Phys.: Condens. Matter **16**, S1177 (2004)

[18] M. J. Castiglione and P. A. Madden, J. Phys.: Condens. Matter **13**, 9963 (2001)

Preprint
UCRL-JC-153550

LAWRENCE
LIVERMORE
NATIONAL
LABORATORY

Melting Of Lithium Hydride Under Presssure

T. Ogitsu, E. Schwegler, F. Gygi, G. Galli

This article was submitted to Physical Review Letters

June 5, 2003

Disclaimer

This document was prepared as an account of work sponsored by an agency of the United States Government. Neither the United States Government nor the University of California nor any of their employees, makes any warranty, express or implied, or assumes any legal liability or responsibility for the accuracy, completeness, or usefulness of any information, apparatus, product, or process disclosed, or represents that its use would not infringe privately owned rights. Reference herein to any specific commercial product, process, or service by trade name, trademark, manufacturer, or otherwise, does not necessarily constitute or imply its endorsement, recommendation, or favoring by the United States Government or the University of California. The views and opinions of authors expressed herein do not necessarily state or reflect those of the United States Government or the University of California, and shall not be used for advertising or product endorsement purposes.

Melting of lithium hydride under pressure

Tadashi Ogitsu, Eric Schwegler, François Gygi, and Giulia Galli
Lawrence Livermore National Laboratory, P.O. Box 808, Livermore, California 94550
(Dated: June 3, 2003)

We have computed the melting line of lithium hydride up to 200 GPa using the two-phase simulation technique coupled with first-principle molecular dynamics. Our predicted melting temperature at high pressures varies slowly with compression, ranging from 2000 to 2450 K at 50-200 GPa pressures. The compressed fluid close to the melting line retains the ionic character of the low pressure molten state, while at higher temperature dynamical hydrogen clustering processes are observed, which are accompanied by changes in the electronic structure.

PACS numbers: 61.20.Ja, 31.15.Ar, 61.25.Qg, 71.15.Pd,62.50.+p,74.62.Fj

Lithium hydride (LiH) is the simplest alkali hydride, possibly the simplest compound material, and its electronic and structural properties have been the subject of extensive investigation [1–5]. Recently, single crystal X-ray diffraction experiments under pressure have been carried out at room temperature for both LiH and LiD. These measurements indicated that LiH (LiD) is stable in the rocksalt structure up to 36GPa (94GPa) [4], while all other alkali hydrides are known to transform to a CsCl structure at lower pressures- 1.2, 2.2-3.1, 4.0 and 28.0-32.0 GPa for CsH, RbH, KH, and NaH, respectively [3, 6]. However, despite the remarkable progress reported in the last decade by both the diamond anvil cell [7] and shock physics communities [8], experimental studies of LiH and, in general, of compressed low-Z materials remains a challenging problem. To date, the high pressure, high temperature phase diagram of LiH is largely known.

Accurate first-principles methods can complement and help interpret high-pressure experiments: they can provide a detailed description of the structural and bonding changes that a material undergoes under extreme conditions, as well as accurate determinations of melting temperatures (T) as a function of pressure (P). However, given the high computational cost in determining phase boundaries, first-principle simulations have been used in only a few cases to compute melting temperatures. Specifically, first-principles free energies calculations using the potential switching method have been used to compute Si [9] and Al [10] melting temperatures, as well as the Fe [11] melting line at high pressure. Unfortunately, these calculations are very demanding because their efficiency depends on the existence of an accurate empirical potential for the specific system and thermodynamic conditions of interest.

Recently, a simple yet accurate method for the determination of melting temperatures has been proposed [12]. This technique, called the two-phase (or coexistence) simulation method, is based on the direct comparison of liquid and solid free energies by performing constant-pressure, constant-temperature (CPT) molecular dynamic (MD) simulations of slabs containing the two phases separated by an interface. To date, the two-phase simulation technique has been applied only in the context of MD simulations using empirical potentials.

In this Letter we have coupled, for the first time, the two-phase simulation method with first-principle molecular dynamics, and we have carried out a study of the melting line of LiH under pressure. Our predicted melting temperatures vary slowly with compression at high pressures, ranging from 2000 to 2450 K in the 50-200 GPa pressure range. In addition, we have investigated the structural and bonding properties of the molten state. Our results show that the compressed fluid close to the melt line retains the ionic character of the low pressure molten state. At higher temperatures, dynamical hydrogen clustering processes are observed, which are accompanied by significant changes in the electronic structure properties.

We performed first-princples simulations using the Car-Parrinello (CP) method [13] and we treated the Li and H nuclei as classical particles. Although quantum effects are important to accurately determine the properties of LiH at zero temperature, e.g. its equilibrium lattice constant, melting temperatures (T_m) and equation of state data at high T are only weakly affected by quantum effects [18]. For example, the difference between the LiH and LiD melting temperature at ambient P is only 2 K. The electron-electron and electron-ion interactions were described within density functional theory, with the Perdue-Burke-Ernzerhof generalized gradient approximation (GGA) [14] for the exchange-correlation energy and potential. A plane-wave basis set and Troullier-Martins pseudopotentials [19] were used with a maximum kinetic energy cut-off of 40 Ry [20]. The simulation cells consisted of 432 atoms (216 atoms in the liquid layer and 216 atoms in the solid layer), and the Γ-point only was used to sample the supercell Brillouin zone. Finite size effects on the lattice constant of the solid are 1% when using 216 atom cells and the Γ point, as compared to a fully converged k-point calculation (4096 k-points with 8 atoms per cell).

In our two-phase simulations, the initial configurations of the solid and liquid phases were generated by single phase constant-volume MD runs; configurations obtained

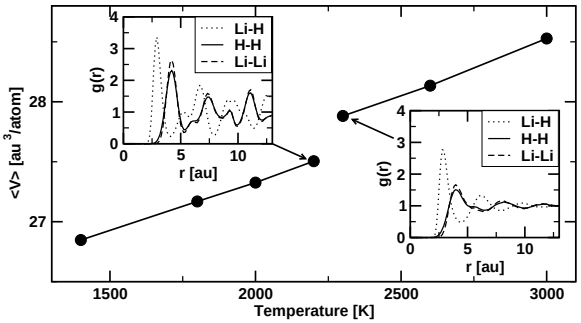

FIG. 1: Computed average volume as a function of temperature at 100 GPa. Solid circles represent data obtained in our simulations, and the lines are guides to the eye. The statistical error bars are smaller than the size of the circles. Insets: pair correlation functions $[g(r)]$ at 2200K (left) and 2300 K (right).(See text).

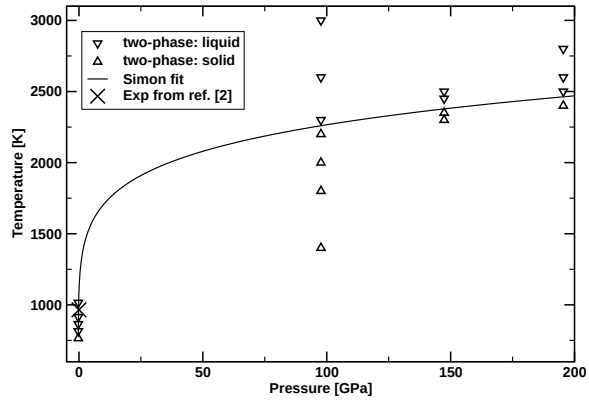

FIG. 2: The predicted melting line of LiH. Our calculated melting temperatures are: $T_m^{0GPa} = 790 \pm 25$K, $T_m^{100GPa} = 2250 \pm 50$K, $T_m^{150GPa} = 2400 \pm 50$K, $T_m^{200GPa} = 2450 \pm 50$K. These values include BO-MD corrections (see text) and the solid line is obtained using a Simon fit of the simulation data: $T_m(P) = 790 \times (1 + (P + 0.28) \times 11.479023)^{0.14812275}$.

in this manner were then combined in a single supercell with a small vacuum area between the solid and the liquid layer. The solid and the liquid phases were heated independently to reduce the strain near the interface. We performed two-phase simulations of LiH at 0, 100, 150, and 200 GPa. In order to assess whether configurations originally prepared in a liquid or solid state would solidify or melt, the mean square displacements of atoms, variations in equilibrium volumes, and changes in pair correlation functions were monitored as a function of the simulation time. For example, in Fig. 1 the discontinuity in the average volume observed between 2200 K and 2300 K at 100 GPa is shown, which is indicative of melting. Calculations of the pair distribution functions $[g(r)]$ and atomic mean square displacements under conditions close to the observed discontinuity confirmed that the samples below and above the discontinuity were indeed in the solid and liquid phase, respectively (see the inset of Fig. 1).

The melting temperature of LiH as a function of pressure predicted by our simulations is shown in Fig. 2. Experimentally, T_m of LiH has been determined only at ambient pressure. Our computed value at P=0, $T_m^{0GPa} = 790 \pm 25$ K, is about 18 % lower than the experimental value, $T_m^{exp} = 965 \pm 2$K [15]. The most likely sources of error are due to the GGA [10] and possibly to inaccuracies introduced by the CP method where the electrons are close to, but not exactly on the Born-Oppenheimer (BO) surface. We have calculated the difference (ΔP_{CP-BO}) between the pressure obtained within CP-MD and BO-MD above and below the computed melting temperatures at the macroscopic densities determined by CP-MD. The values of ΔP_{CP-BO} at 0, 100, 150, and 200 GPa, are $-0.28\pm0.03, -2.33\pm0.11, -2.62\pm0.19, -4.01\pm0.17$ GPa, respectively. Therefore, CP dynamics leads to a few percent underestimate of T_m at all pressures; we estimate that the error in T_m at low P is approximately 5 % due to inaccuracies introduced by CP dynamics, and the remainder due to the GGA. It is interesting to note that all of the melting temperatures calculated within LDA or GGA reported in the literature underestimate the corresponding experimental values at low pressure [9–11], e.g. 16 % in Al and 20 % in Si. This effect may be due to the general tendency of the LDA to overestimate the stability of the liquid phase with respect to the solid state in cases where upon melting the electronic charge density tend to become more homogeneous.

As it is seen in Fig. 2, the melting curve is very steep below 20-30 GPa and becomes rather flat between 50 and 200 GPa. A similar behavior of T_m as a function of P has been observed for other ionic systems, e.g. LiF, NaCl, KBr, KCl, and CsI by Bohler *et al.* [16, 17] using laser heated diamond-anvil cell experiments.

We now turn to the discussion of the structural and bonding properties of the liquid. The pair correlation functions at low and high pressure, at four different (P, T) conditions are shown in Fig. 3; in all cases correlation functions characteristic of a molten salt are observed. We find that the Li-H ionic bond is very stiff and its length depends weakly on pressure, as indicated by the position of the first peak of $g^{\text{Li-H}}(r)$ which does not scale with the cubic root of the density, $a = \sqrt[3]{\rho}$. On the other hand, H-H and Li-Li distances do scale with a. The coordination numbers defined by the integration of $g^{ij}(r)$ up to the first minimum indicate that while the coordination of H around Li does not change under pressure, *i.e.,* it remains constant at about 6, the H-H and Li-Li coordinations increase from 12 at ambient P to about 20 at 100 GPa. An additional indication that, in spite of some structural changes in the second and third neighbor coordination shell, the ionic character of the Li-H bond is retained in the high pressure fluid comes from the computed diffusion coefficients of Li and H. The results obtained at

100 GPa, close to the melting temperature are shown in Fig. 4. It is seen that Li and H diffusion coefficients are very similar, in spite of the ratio between their masses, $m_{\rm Li} : m_{\rm H} \approx 1 : 7$, which is clearly reflected in their respective velocity distribution (see Fig. 4b). The similarity in the Li and H diffusion coefficient indicates that the motion of neighboring lithium and hydrogen atoms are strongly correlated because of their ionic bond, and thus the two atomic species diffuse together for long periods of time. The fast motion of hydrogen atoms is mostly a vibrational and rotational/librational motion around a neighboring lithium atom and it does not contribute to the diffusion constant.

While close to the melting line, over the pressure range considered here, we have found that the fluid is characteristic of an ionic liquid. However, when the temperature is raised above melting, hydrogen cluster formation processes are observed, which perturbs the ionic character of the fluid. As shown in the insets of Fig. 3b and 3d, $g^{\rm H\text{-}H}(r)$ has a small but finite distribution at $r = 1.4$ au, which corresponds to the equilibrium bond length of the H_2 molecule. We have carried out single-phase constant temperature constant volume MD runs using the density at 0 GPa and 0 K, and raised the temperature to 2200K, where dynamical H_2 molecule formation and dissociation process are observed. By quenching the system down to 1015 K and releasing the pressure to 0 GPa, we obtained a fluid with a small number of H_2 molecules. One of the H_2 molecules persisted over more than 10 ps of simulation. At higher P and T (100 GPa, 3000 K), we also found dynamical clustering processes taking place. However, after quenching the system to 2300 K, no hydrogen clusters were found. This indicates that H_2 formation is likely to take place only at high T. It also suggests that the H_2 molecules observed at 0 GPa might depend on the initial configuration. A simulation at 0 GPa and 1015 K starting from a configuration at 2300 K and 100 GPa (where no hydrogen clusters are present) was then performed and no H_2 molecules were observed over 4 ps of simulation. In addition, we have computed the average energies of the samples at 0 GPa and 1015 K with and without H_2 molecules and found that the presence of H_2 molecules raises the total energy of the fluid by 3.0 ± 0.3 eV/cell, indicating that the H_2 molecules are most-likely in a meta-stable state at ambient pressure and low T ($\simeq$ 1000 K).

The charge state of the H_2 molecule observed in the fluid raises very simple yet fundamental questions. When the system is in an ionic configuration, Li atoms are positively charged and H atoms are negatively charged. If a pair of H atoms formed a molecule without changing the charge state of the original atoms, the anti-bonding level of the H_2 molecule would have to be occupied and the molecule would be unstable. Alternatively, if the excess electrons on H_2 are transferred to the bulk fluid, one may expect the overall ionicity of the liquid would be weakened, possibly causing the system to become less stable.

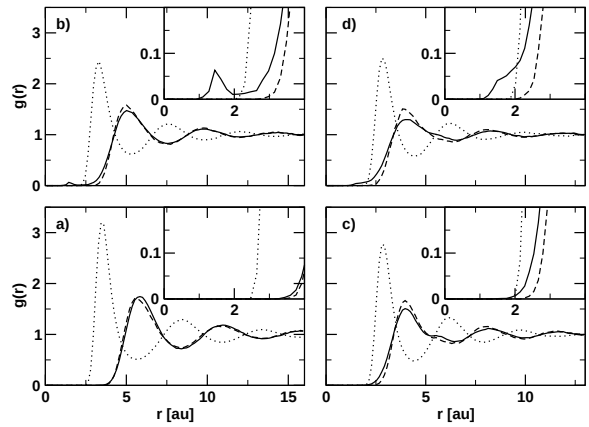

FIG. 3: The pair correlation functions of liquid LiH at a) 1015 K and 0 GPa, b) 2200K and 12.9 ± 0.1 GPa, c) 2300 K and 100 GPa, d) 3000 K and 100 GPa. H-H, solid line; Li-H, dotted line; Li-Li dashed line. Inset: The region below 4 au is enlarged to show the probability of hydrogen cluster formation.

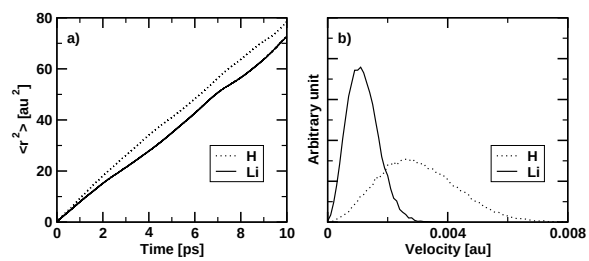

FIG. 4: a) The mean square displacements of lithium and hydrogen. b) The velocity distributions of lithium and hydrogen.

We have calculated the electronic structure of liquid LiH with and without H_2 at 0 GPa and 1015 K, and have analyzed the effect of H_2 molecule formation on the electronic structure. Approximately 50 atomic configurations were randomly selected from the MD runs, and the eigenstates calculated using the preconditioned steepest descent method combined with a subspace diagonalization scheme.

The calculated electronic density of states (EDOS) of the fluids with and without H_2 are shown in Fig. 5a. In the EDOS without H_2, a clear energy gap between the valence and the conduction band is found, while in the EDOS with H_2, a pair of new levels appear below the valence band bottom (VBB) and above the valence band top (VBT). The level below the VBB is found to be a bonding state of the H_2 molecule, while the one above the VBT is a delocalized state. No eigenstates with an appreciable amplitude on the H_2 molecule has been found except for the H_2 bonding state, indicating that the charge state of the H_2 molecule is close to neutral.

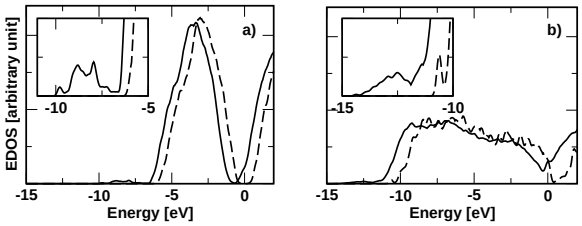

FIG. 5: Time averaged density of states, at a) 0GPa and 1015 K (solid line denotes EDOS with H_2 molecules and dashed line denotes EDOS without H_2 molecules), b) 100GPa (solid line denotes EDOS at 3000 K and dashed line denotes EDOS at 2300 K). Inset: The region below the bulk valence band is enlarged to show the states associated with hydrogen cluster (molecule). The scale of the Y-axis are identical.

The electron released to the fluid upon formation of an H_2 molecule affects the overall ionicity of the liquid and it is responsible for a volume expansion. In our simulations we observed $\langle V^{0GPa}_{H_2} \rangle = 94.0648 \pm 0.259[au^3/atom]$ and $\langle V^{0GPa}_{No\ H_2} \rangle = 93.3704 \pm 0.097[au^3/atom]$.

The EDOS at 100 GPa are shown in Fig. 5b. At 2300 K, where H clustering does not take place, a clear energy gap is found and no states below the VBB are seen, while at 3000 K a significant amount of states below the VBB and around the Fermi level are observed. By inspecting the eigenstates, the levels below the VBB are identified as states related to H clusters, while those above the VBT are rather featureless. These levels range from the valence to the conduction band, without a clear gap[21].

In conclusion, we have coupled the two-phase simulation technique with first-principle molecular dynamics for the first time, and have computed the melting line and the structural and bonding properties of LiH under pressures up to 200 GPa. Our results show that with moderate size supercells (about 500 atoms) and relatively short time scales (about 5 ps), melting temperatures can be accurately computed as a function of compression from first-principles. This opens the way to systematic studies of melting temperatures using DFT, for differently bonded systems, under various thermodynamic conditions. Our simulations show that while LiH retains its ionic character in the liquid close to the melting curve, dynamical H clustering processes occur at higher T. We propose that the H clustering process could be evidenced experimentally by an increase of the liquid volume as a function of T, as well as by photoemission experiments, although this may be prohibitively difficult to carry out in a hot, compressed fluid. Finally we note that, although the melting curves of alkali halides are located significantly higher in P than that of LiH, the behavior of the LiH melting line is similar to that of alkali halides, where a sharp rise in the low P regime is usually observed, followed by a flattening at high P.

The authors acknowledge Prof. Anatoly Belonoshko for stimulating discussions. This work was performed under the auspices of the U.S. Dept. of Energy at the University of California/ LLNL under contract no. W-7405-Eng-48.

[1] E. E. Shpilrain, K. A. Yakimovich, M. E. Melnikova, and A. Y. Polishchuk, *Thermophysical Properties of Lithium Hydride, Deuteride, and Tritide and of Their Solutions with Lithium* (American Institute of Physics, 1987).
[2] J. Hama, K. Suito, and N. Kawakami, Phys. Rev. B **39**, 3351 (1989).
[3] R. Ahuja, O. Eriksson, and B. Johanssen, Physica B **265**, 87 (1999).
[4] P. Loubeyre, R. L. Toullec, M. Hanfland, L. Ulivi, F. Datchi, and D. Hausermann, Phys. Rev. B **57**, 10403 (1998).
[5] S. Lebègue, M. Alouani, B. Arnaud, and W. E. Pickett, Submited to Europhsics Letters (2003).
[6] H. D. Hochhemer, K. Strossner, and W. Honle, Z. Phys. Chemie Neue Folge **143**, 139 (1985). S. J. Duclos, Y. K. Vohra, and A. L. Ruoff, Phys. Rev. B **36**, 7664 (1987).
[7] E. Gregoryanz, A. F. Goncharov, K. Matsuishi, H.-k. Mao, and R. J. Hemley, Phys. Rev. Lett. **90**, 175701 (2003). P. Loubeyre, F. Occelli, and R. LeToullec, Nature **416**, 613 (2002). V. Iota and C.-S. Yoo, Phys. Rev. Lett. **86**, 5922 (2001).
[8] M. D. Knudson, D. L. Hanson, J. E. Bailey, C. A. Hall, and J. R. Asay, Phys. Rev. Lett. **90**, 035505 (2003).
[9] O. Sugino and R. Car, Phys. Rev. Lett. **74**, 1823 (1995).
[10] L. Vočadlo and D. Alfè, Physical Review B **65**, 214105 (2002).
[11] D. Alfè, M. J. Gillan, and G. D. Price, Nature **401**, 462 (1999).D. Alfè, G. D. Price, and M. J. Gillan, Phys. Rev. B **65**, 165118 (2002).
[12] A. Belonoshko, Geochim. Cosmochim. Acta **58**, 4039 (1994). O. Tomagnini, F. Ercolessi, S. Iarlori, F. D. D. Tolla, and E. Tosatti, Phys. Rev. Lett. **76**, 1118 (1996).
[13] R. Car and M. Parrinello, Phys. Rev. Lett **55**, 2471 (1985).
[14] J. P. Perdew, K. Burke, and M. Ernzerhof, Phys. Rev. Lett. **77**, 3865 (1996).
[15] C. E. Messer and I. S. Levy, Inorg. Chem. **4**, 543 (1964).
[16] R. Boehler, M. Ross, and B. Boercker, Phys. Rev. B **53**, 556 (1996).
[17] R. Boehler, M. Ross, and D. B. Boercker, Phys. Rev. Lett. **78**, 4589 (1997).
[18] See, for example, page 12, 55, and 56 of Ref. [1]
[19] N. Troullier and J. L. Martins, Phys. Rev. B **43**, 1993 (1991). Pseudopotentials with s-nonlocal, p-local, and s-local, p,d-nonlocal were used for H and Li, respectively.
[20] Constant resolution in the simulations was achieved with a 45 Ry cutoff energy combined with a three dimensional well potential in momentum space with a 40 Ry radius to mimic the constant cutoff energy at 40 Ry.
[21] GGA (LDA) is known to underestimate the electronic band gap of semiconductors and insulators and thus only qualitative statements about the comparison between samples with and without hydrogen molecules are reported here. More quantitative studies of band gap closure in the liquid under pressure would require methods beyond the GGA of DFT.

UCRL-JRNL-206079

LAWRENCE
LIVERMORE
NATIONAL
LABORATORY

Evidence Towards A Quantum Fluid Of Metallic Hydrogen From First-principles Calculations

S. Bonev, E. Schwegler, T. Ogitsu, G. Galli

August 16, 2004

Nature

Disclaimer

This document was prepared as an account of work sponsored by an agency of the United States Government. Neither the United States Government nor the University of California nor any of their employees, makes any warranty, express or implied, or assumes any legal liability or responsibility for the accuracy, completeness, or usefulness of any information, apparatus, product, or process disclosed, or represents that its use would not infringe privately owned rights. Reference herein to any specific commercial product, process, or service by trade name, trademark, manufacturer, or otherwise, does not necessarily constitute or imply its endorsement, recommendation, or favoring by the United States Government or the University of California. The views and opinions of authors expressed herein do not necessarily state or reflect those of the United States Government or the University of California, and shall not be used for advertising or product endorsement purposes.

arXiv:cond-mat/0410425 v1 17 Oct 2004

A quantum fluid of metallic hydrogen suggested by first-principles calculations

Stanimir A. Bonev*, Eric Schwegler, Tadashi Ogitsu & Giulia Galli

Lawrence Livermore National Laboratory, University of California, Livermore, California 94550

It is generally assumed[1,2,3] that solid hydrogen will transform into a metallic alkali-like crystal at sufficiently high pressure. However, some theoretical models[4,5] have also suggested that compressed hydrogen may form an unusual two-component (protons and electrons) metallic fluid at low temperature, or possibly even a zero-temperature liquid ground state. The existence of these new states of matter is conditional on the presence of a maximum in the melting temperature versus pressure curve (the 'melt line'). Previous measurements[6,7,8] of the hydrogen melt line up to pressures of 44 GPa have led to controversial conclusions regarding the existence of this maximum. Here we report *ab initio* calculations that establish the melt line up to 200 GPa. We predict that subtle changes in the intermolecular interactions lead to a decline of the melt line above 90 GPa. The implication is that as solid molecular hydrogen is compressed, it transforms into a low-temperature quantum fluid before becoming a monatomic crystal. The emerging low-temperature phase diagram of hydrogen and its isotopes bears analogies with the familiar phases of ^{3}He and ^{4}He, the only known zero-temperature liquids, but the long-range Coulombic interactions and the large component mass ratio present in hydrogen would ensure dramatically different properties[9,10].

The possible existence of low-temperature liquid phases of compressed hydrogen has been rationalized with arguments based on the nature of effective pair interactions and of the quantum dynamics at high density, resulting in proton-proton correlations insufficient for the stabilization of a crystalline phase[5]. But so far there has been no conclusive evidence establishing whether hydrogen metallizes at low temperature as a solid (the more widely accepted view to date) or as a liquid. Measurements and theoretical predictions of the near-ground state high-pressure phases[3] of hydrogen have proven to be difficult because of the light atomic mass, significant quantum effects and strong electron-ion interactions. In this regard, the finite temperature liquid-solid phase boundary predicted here is especially valuable for understanding the manner in which hydrogen metallizes.

The appearance of a maximum melting temperature in hydrogen is in itself a manifestation of an unusual physical phenomenon. The few systems with a negative melt slope involve either open crystalline structures, such as water and graphite, or in the case of closed packed solids, a promotion of valence electrons to higher orbitals upon compression (6s to 5d in cesium[11], for example). In these cases, the liquid is denser than the solid when they coexist, possibly because of structural or electronic transitions taking place continuously in the liquid, as a function of pressure, but only at discrete pressure intervals in the solid.

In contrast, recent experiments[8] have shown that hydrogen phase I – a solid structure with rotationally-free molecules associated with the sites of a hexagonal closed packed (hcp) lattice – persists below the liquid transition up to at least 150 GPa, i.e. well beyond the melt curve maximum predicted here. The promotion of electrons to higher orbitals in hydrogen can also be ruled out because of the prohibitive high energy involved. Alternatively, it has been suggested that dissociation in the fluid, either gradual[7] or following a first-order liquid-liquid (LL) phase transition[12,13], may be the origin of a maximum in the melt line. This idea is not supported by our results. Instead, we explain the physical origin of the maximum in terms of changes in the *intermolecular* interactions – a mechanism significantly different from that expected from familiar phenomenological models.

The approach taken here to compute the melt line is one of direct simulation of the melting process. Hysteresis effects of super-heating or super-cooling during the phase transition are avoided by simulating solid and liquid phases in coexistence. The validity of this method

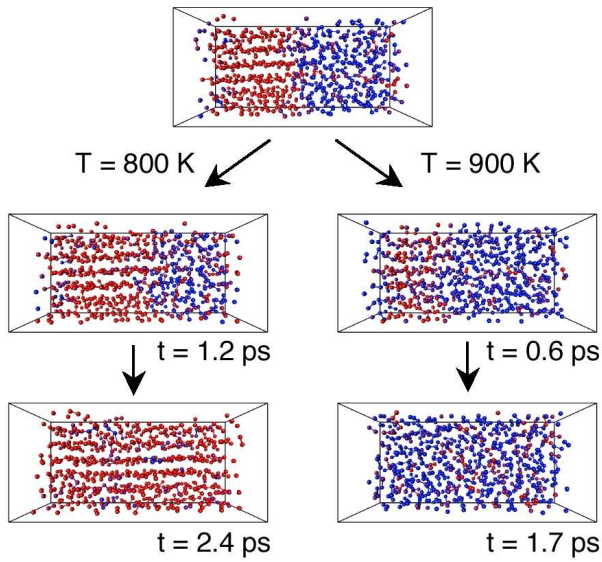

FIG. 1: Snapshots from two-phase MD simulations at P = 130 GPa and temperatures below and above the melting temperature. A quantitative assessment of the instantaneous local order environment around each molecule has been performed as described in Ref. 17, and compared with single-phase solid and liquid simulations. Molecules are coloured according to the arrangement of their nearest neighbours, red and blue representing configurations uniquely characteristic of the hcp solid and liquid at the given P and T, respectively (the Q_4 order parameter[17] has been used for the colour map). The systems reach equilibrium at the target average temperatures (800 and 900 K) over a time interval of $\sim$ 0.5 ps, which is followed by periods of coexistence lasting from 1 to several picoseconds. The phase transitions are observed by monitoring changes in the diffusion constants, pair correlation functions, specific volumes and local order parameters. In addition, some noticeable correlations between temperature and diffusion variations indicate the exchange of latent heat.

is then assessed by reducing size effects in such a way that realistic thermodynamic processes can be mimicked. This technique, known as two-phase simulation, has been mostly applied with model potentials[14], thus allowing the simulation of large systems, and only recently it was demonstrated[15,16] that implementations within the framework of first principles molecular dynamics (MD) are feasible.

Two-phase simulations (Fig. 1) are performed for various pressure and temperature conditions to predict the melt curve of hydrogen up to 200 GPa (Fig. 2). As discussed in Refs. 7 and 8, the experimental data available up to 44 GPa can be equally well fitted with several empirical melt equations, leading to qualitatively different conclusions regarding the further rise or fall of the phase boundary. Our results at 50 GPa compare favourably with recent measurement[8], and the calculations at 130 and 200 GPa predict a negative slope in this pressure region.

Previous first-principles calculations[12,19] indicated the existence of a sharp transition from molecular to non-molecular fluid, thus raising the possibility that the melt curve maximum is a liquid-liquid-solid triple point. We therefore studied the properties of the liquid at temperatures above melting. In our simulations, we do find a first-order liquid-liquid phase transition from molecular to dissociating fluid, but this occurs at temperatures higher than those of the melting line; at 200 GPa, the liquid-liquid transition takes place between 900 and 1,000 K (Fig. 2). Thus, in the entire pressure range considered here, the liquid remains molecular below 900 K, with molecules stable over the simulation times of several picoseconds. We emphasize that on heating above a critical temperature, the transition to a non-molecular fluid takes place very rapidly, over a couple of hundred femtoseconds of simulation time. When the fluid is subsequently quenched, the molecules recombine and the system reverts to the molecular state. Therefore, we conclude that the change from a positive to a negative melt line slope happens gradually and we emphasize that it is not directly related to molecular dissociation. However, extrapolations of the melt line and the liquid-liquid phase transition indicate a triple point at $\sim$ 300 GPa and 400 K. Above this pressure, the solid is expected to melt into a metallic liquid.

To estimate the errors originating from finite system size effects, we have computed the ground state pressure and energy for different size simulation cells sampled at the the Γ-point and with a 2x2x2 **k**-point mesh. The pressure and energy *differences* between the solid and the liquid are converged to within 0.3 GPa and 1 meV

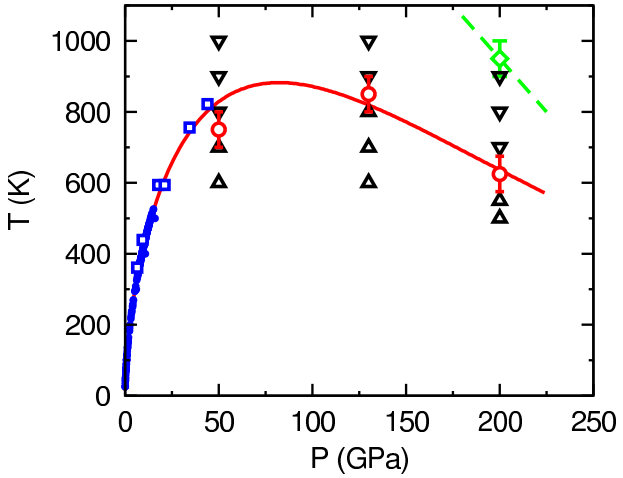

FIG. 2: Melt curve of hydrogen predicted from first principles MD. The filled circles are experimental data from Refs. 6 and 7 and references therein, and the open squares are measurements from Ref. 8. Triangles indicate two-phase simulations where solidification (up) or melting (down) have been observed, and bracketed melting temperatures (T_m) are represented by open circles. As the phase boundary is approached, the period of coexistence increases and eventually the outcome becomes dependent on the choice of simulation parameters. This degree of arbitrariness is reflected in the error bars of T_m, which also include the standard deviation of the temperatures collected during the MD simulations. All experimental and theoretical points are given equal weight and fitted with a Kechin melt equation[18] (solid line in the figure): $T_m = 14.025\,(1+P/a)^b \exp(-cP)$ K, where P is in units of GPa, $a = 0.030355$, $b = 0.59991$, and $c = 0.0072997$. The open diamond marks the liquid-liquid transition from molecular to non-molecular fluid at 200 GPa, and the estimated slope of this phase boundary is given by the dashed line. The error bar on the diamond symbol indicates the hysteresis effects during the simulation of the liquid-liquid transition.

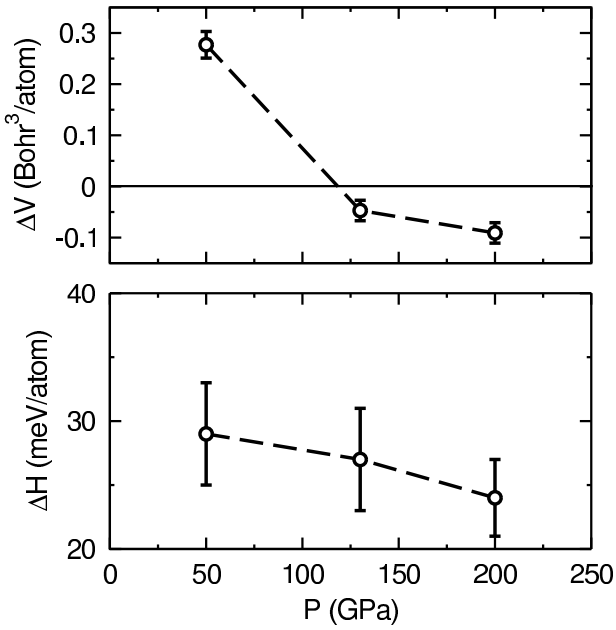

FIG. 3: Difference of the specific volumes (ΔV) and enthalpies (ΔH) between the liquid and solid phases at the melting temperatures determined from the two-phase simulations. The reported uncertainties include standard deviations collected during the MD simulations and observed size effects from singe-phase simulations with 360 and 768 atom supercells. The data are used to compute melt slopes from the Clausius-Clapeyron equation: $dT_m/dP = T_m \Delta V/\Delta H$; the values obtained for 50, 130 and 200 GPa are (6.5 ± 1.2), (-1.4 ± 0.6) and (-2.3 ± 0.6) K/GPa, respectively. For comparison, the slopes from the melt line fit in Figure 2 are 3.9, -2.2 and -2.7 K/GPa, but we note that these are weighted heavily by the experimental data, especially at lower pressure.

per ion, and the estimated errors are included in Fig. 3. A question that remains to be answered is whether the size of the system considered here is sufficient to simulate liquid-solid coexistence. To address this, we carried out MD simulations of single-phase solid and liquid hydrogen at the melting temperatures determined in the two-phase simulations. The differences in the specific volumes and enthalpies obtained in this way (Fig. 3) are then used to compute the melt slopes using the Clausius-Clapeyron equation. The agreement with the results from two-phase simulations gives us confidence that the computed melt curve is thermodynamically consistent.

We also discuss the validity of the principal approximations in our theoretical method: (1) adiabatic interactions, (2) the generalized gradient approximation (GGA) for the exchange-correlation energy, and (3) classical treatment of ion motion. Electron-phonon interactions are significant in the solid phase when the direct band gap is comparable with the phonon frequencies; an event that eventually occurs at high densities. But at 200 GPa and 600 K – the conditions examined here where the electron-phonon coupling is expected to be most pronounced – the GGA band gap is still ~ 2 eV. We note that the GGA tends to systematically underestimate band gaps; this has been shown for various materials, including hydrogen[20]. However, because the highest vibrational frequencies in hydrogen are ~ 0.5 eV, the computed GGA band gap – a lower bound to the actual value – is already sufficient to establish that non-adiabatic effects are indeed negligible.

Local density approximations are also expected to favour the phase with more delocalised electrons; previous studies have shown a consistent tendency of the GGA to underestimate melting temperatures, such as those of lithium hydride[15] and aluminium[16]. Here, this effect is expected to be very small because the molecular bonding properties and the atomic coordination differ little in the solid and liquid phases. This also implies that the zero-point energy bound in the vibron motion is similar in the two phases. Indeed, velocity-velocity autocorrelation analysis carried out on our MD trajectories shows that vibron frequency distributions (containing all vibrational modes) differ by less than 10 cm^{-1} in the solid and the liquid between 50 and 200 GPa. In addition, we have computed the first-order quantum correction to the ionic free energies. It is given by the Wigner-Kirkwood formula, $\Delta F = \hbar^2/(24k_B^2T^2)\sum_i\langle\mathbf{F}_i^2\rangle/m_i$, where the average is over the classical ensemble, and $\mathbf{F}_i$ and m_i are the ionic forces and masses. The *difference* in the quantum corrections for the two phases obtained in this way at pressures of 50, 130 and 200 GPa remains less than 2 meV for temperatures near the computed melt curve.

We now turn our attention to the physical origin of the maximum in the melt curve of hydrogen. The transition from an ordered to a disordered state is governed by the relative importance of entropy and energy. At high pressure, the interactions become mostly repulsive, and it is reasonable to expect that a deviation from a crystalline arrangement becomes progressively more unfavourable in terms of enthalpy. This is indeed the case for most materials, as is reflected in the positive slopes of their melt curves. On the other hand, attractive many-body interactions can soften the steep increase of the repulsive forces at high density[21,22]. Although, in principle, such a softening opens up the possibility for a melt curve maximum[23], it does not appear to be a sufficient condition for its existence. Indeed, softening of the repulsive part of the pair potentials has been observed for a number of materials for which there is no experimental indication of a melt line turnover. As will be shown below, the physics behind the unique melt curve of hydrogen is related to the *different rate* at which the repulsive interactions (at intermolecular range) are weakened in the solid and liquid phases as a function of pressure.

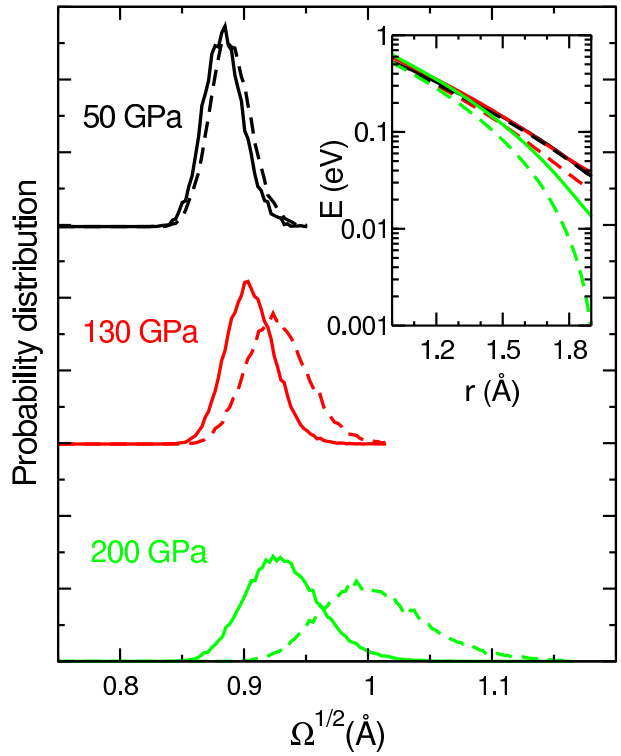

FIG. 4: The probability distribution of MLWF spreads[24] at T=700 K and P=50 (black curves), 130 (red curves) and 200 GPa (green curves). The solid and dashed curves correspond to distributions collected from the solid and liquid phases, respectively. The inset shows the effective hydrogen-hydrogen potentials obtained directly from the simulation trajectories with the force-matching procedure described in Ref. 26 (the same coloring has been used). As the pressure is increased, the spreads of the MLWF are shown to increase faster in the liquid than in the solid phase. In addition, effective potentials soften more quickly in the liquid than in the solid phase at the nearest neighbor molecular separation distance. Note that the potentials at 50 GPa in the liquid and solid phases, and at 130 GPa in the solid phase, are indistinguishable on this scale.

To investigate how many-body interactions give rise to repulsive force softening in the liquid and the solid, we have performed an analysis based on maximally-localized Wannier functions (MLWF). These functions have been shown[24] to provide an intuitive description of chemical bonds in condensed phases and they have recently been used[25] to investigate the infrared activity of candidate structures of hydrogen phase III. We have computed MLWF along the 700 K isotherm, at various pressures, and find that their spreads (Fig. 4) increase faster in the

fluid than in the solid, as the system is compressed. Importantly, the differences in the two phases come from the tails of the MLWF, while their profiles around the centres of the molecular bonds remain nearly the same. Therefore, the large MLWF spread observed in the high-pressure fluid comes from the increased overlap of the molecular orbitals, here represented by the MLWF. Because the specific volumes of the solid and the liquid are very similar under the conditions examined here, the physical origin of the larger spread in the fluid can be attributed to the disorder in the liquid phase. Furthermore, the tails of the MLWF in the fluid are characterized by an asymmetry, which can be viewed as an effective intermolecular charge transfer, giving rise to an enhanced infrared activity in the liquid phase.

The properties of the MLWF found in our calculations are indicative of the behaviour of repulsive interactions in the solid and liquid as a function of pressure. Effective hydrogen-hydrogen pair potentials derived from our *ab initio* MD trajectories using a force matching technique[26] are displayed in the inset of Fig. 4. As in the MLWF behaviour, we observe a stronger softening of the potential in the liquid than in the solid. Our Wannier function analysis indicates that this increased softening is the result of charge transfer processes, enhanced by disorder, which appear to have a qualitative character similar to those proposed in Ref. 27 for phase III of solid hydrogen. We also note that the attenuation of repulsive interactions observed here in the solid phase correlates well with the analysis of Raman spectroscopic data[28], which has indicated softening of the effective intermolecular force constants above ∼100 GPa.

To summarize, we have predicted the melt curve of hydrogen between 50 and 200 GPa from first principles. Above approximately 82 GPa, the melt line has a negative slope – a phenomenon that we have related to softening of the intermolecular interactions, which occur at a faster rate in the liquid than in the solid, as a function of pressure. Our results provide strong evidence that above ∼300 GPa the solid melts into a metallic liquid and that a low-temperature metallic quantum fluid will exist at pressures near 400 GPa. Although we have only directly probed temperatures as low as 600 K, our conclusions are likely to hold at lower temperatures as well. Indeed, quantum ion motion usually favours phases with lower ion-ion correlations, which would further stabilize the low-temperature liquid phase found here. In addition, our findings are consistent with pressure estimates from experiments where hydrogen is expected to metallize[3,29]. Finally, we note that the observed increase in MLWF spreads when going from the high-pressure solid to the molecular liquid phase points at the presence of dynamically-induced intermolecular charge transfer (dipole moments); this indicates that the transition from solid to liquid at high pressure is accompanied by an increase of the hydrogen infrared absorption. Therefore, we propose that measurements of infrared activity could be used to verify experimentally the predicted turnover of the melt curve.

Methods

Molecular dynamics

Our *ab initio* MD simulations are carried out with the GP code, written by F. Gygi, and using the Car-Parrinello (CP) method[30]; the many-body electron problem was solved quantum-mechanically within the generalized gradient approximation[31] of density functional theory, while the ions are propagated classically (the validity of this approximation for the problem at hand is discussed in the text). The actual calculations are performed for deuterium instead of hydrogen. The reason for this is that in the classical-ion picture, for the quantities of relevance here there is no distinction between hydrogen and its isotopes, but the substitution with heavier ions allows us to integrate the equations of motion with reasonably large time steps: 2 and 3 a.u. (1 a.u. = 0.0242 fs) depending on the density. Furthermore, we use a Γ-point sampling of the Brillouin zone, Troullier-Martins pseudopotentials, and 60 Ry energy cut-off for the plane wave expansion of the Kohn-Sham orbitals. The accuracy and transferability of our pseudopotential has previously been extensively tested[19]. We have explicitly verified that the electrons remain near the Born-Oppenheimer surface throughout the simulations by comparing pressures determined in the CP runs with those determined by fully optimizing wavefunctions for the same ionic trajectories. The use of CP-MD results in a systematic shift of about 0.5 GPa both in the solid and liquid phases.

Two-phase simulations

We perform the two-phase simulations by equilibrating solid (in the hcp structure) and liquid phases separately in 360-atom supercells with fixed geometry and applied periodic boundary conditions. The atomic arrangements obtained in this way are then merged, and the liquid and solid parts of the resulting 720-atom supercells are also heated independently to reduce the strain near the newly-formed interface. The whole equilibration process typically lasts for several picoseconds of simulation time. The MD runs of coexisting phases are then performed in the $N-P-T$ ensemble (constant number of particles, pressure and temperature respectively). The actual system being simulated initially represents semi-infinite alternating slabs (by applying periodic boundary conditions) of solid and liquid, but by the end of the runs only one of the two phases, the one that is stable at the chosen P and T, fills the entire volume.

* Present address: Department of Physics, Dalhousie University, Halifax, Nova Scotia B3H 3J5, Canada.

[1] Wigner, E. & Huntington, H. B. On the possibility of metallic modifications of hydrogen. *J. Chem. Phys.* **3**, 764-770 (1935).

[2] Ashcroft, N. W. Metallic hydrogen: A high-temperature superconductor? *Phys. Rev. Lett.* **21**, 1748-1799 (1968).

[3] Mao, H. K. & Hemley, R. J. Ultrahigh-pressure transitions in solid hydrogen. *Rev. Mod. Phys.* **66**, 671-692 (1994).

[4] Brovman, E. G., Kagan, Yu. & Kholas, A. Properties of

metallic hydrogen under pressure. *Sov. Phys. JETP* **35**, 783-792 (1972).

[5] Ashcroft, N. W. The hydrogen liquids. *J. Phys.: Condens. Matter* **12**, A129-137 (2000).

[6] Diatschenko, V. *et al.* Melting curves of molecular hydrogen and molecular deuterium under high pressures between 20 and 373 K. *Phys. Rev B* **32**, 381-389 (1985).

[7] Datchi, F., Loubeyre, P. & LeToullec, R. Extended and accurate determination of the melting curves of argon, helium, ice (H_2O) and hydrogen (H_2). *Phys. Rev B* **61**, 6535-6546 (2000).

[8] Gregoryanz, E., Goncharov, A. F., Matsuishi, K., Mao, H.-k., & Hemley, R. J. Raman spectroscopy of hot dense hydrogen. *Phys. Rev. Lett.* **90**, 175701 (2003).

[9] Ashcroft, N. W. Hydrogen at high density. *J. Phys. A: Math. Gen.* **36**, 6137-6147 (2003).

[10] Babaev, E., Sudbø, A., & Ashcroft N. W. A superconductor to superfluid phase transition in liquid metallic hydrogen. *Nature* **431**, 666-669 (2004).

[11] Jayaraman, J., Newton, R. C. & McDonough, J. M. Phase relations, resistivity, and electronic structure of cesium at high pressure. *Phys. Rev.* **159**, 527-533 (1967).

[12] Scandolo, S. Liquid-liquid phase transition in compressed hydrogen from first-principles simulations. *PNAS* **100**, 3051-3053 (2003).

[13] Kechin, V. V. Melting of metallic hydrogen at high pressure. *JETP Lett.* **79**, 46-49 (2004).

[14] Morris, J. R., Wang, C. Z., Ho, K. M. & Chan, C. T. Melting line of aluminum from simulations of coexisting phases. *Phys. Rev. B* **49**, 3109-3115 (1994).

[15] Ogitsu, T., Schwegler, E., Gygi, F. & Galli, G. Melting of lithium hydride under pressure. *Phys, Rev. Lett.* **91**, 175502 (2003).

[16] Alfe, D. First-principles simulations of direct coexistence of solid and liquid aluminum. *Phys. Rev. B* **68**, 064423 (2003).

[17] Steinhardt, P. J., Nelson, D. R. & Ronchetti M. Bond-orientational order in liquids and glasses. *Prys. Rev. B* **28**, 784-805 (1983).

[18] Kechin, V. V. Melting curve equations at high temperature. *Phys Rev. B* **65**, 052102 (2001).

[19] Bonev, S. A., Militzer, B. & Galli, G. Ab initio simulations of dense liquid deuterium: Comparison with gas-gun shock-wave experiments. *Phys. Rev. B* **69**, 104101 (2004).

[20] Chacham, H., Zhu, X. & Louie, S. G. Pressure-induced insulator-metal transitions in solid xenon and hydrogen: A first-principles quasiparticle study. *Phys. Rev. B* **46**, 6688-6699 (1992).

[21] Hemley, R. J. *et al.* Equation of state of solid hydrogen and deuterium from single-crystal x-ray diffraction to 26.5 GPa. *Phys. Rev. B* **42**, 6458-6470 (1990).

[22] Nagao, K., Bonev, S. A., Bergara, A. & Ashcroft, N. W. Enhanced Friedel structure and proton pairing in dense solid hydrogen. *Phys. Rev. Lett.* **90**, 035501 (2003).

[23] Yoshida, T. & Kamakura S. Liquid-solid transitions in systems of soft repulsive forces. *Progr. Theor. Phys.* **52**, 822-838 (1972).

[24] Marzari, N & Vanderbilt, D. Maximally localized generalized Wannier functions for composite energy bands. *Phys. Rev. B* **56**, 12847-12856 (1997).

[25] Souza, I., Martin, R. M., Marzari, N., Zhao, X. & Vanderbilt, D. Wannier-functional description of the electronic polarization and infrared absorption of high-pressure hydrogen. *Phys. Rev. B* **62**, 15505-15519 (2000).

[26] Izvekov, S., Parrinello, M., Burnham, C. J., & Voth, G. A. Effective force fields for condensed phase systems from ab initio molecular dynamics simulations: A new method for force-matching. *J. Chem. Phys.* **120**, 10896-10913 (2004).

[27] Hemley, R. J., Soos, Z. G., Hanfland & M., Mao, H. K. Charge-transfer states in dense hydrogen. *Nature* **369**, 384-387 (1994).

[28] Moshary F., Chen N. H. & Silvera I. F. Pressure dependence of the vibron in H_2, HD, and D_2: Implications for inter- and intramolecular forces. *Phys. Rev. B* **48**, 12613-12619 (1993).

[29] Loubeyre, P., Occelli, F. & LeToullec, R. Optical studies of solid hydrogen to 320 GPa and evidence for black hydrogen. *Nature* **416**, 613-617 (2002).

[30] Car, R. & Parrinello, M. Unified approach for molecular dynamics and density-functional theory. *Phys. Rev. Lett.* **55**, 2471-2474 (1985).

[31] Perdew, J. P., Burke, K. & Ernzerhof M. Generalized gradient approximation made simple. *Phys. Rev. Lett.* **77**, 3865-3868 (1996).

Acknowledgments We gratefully acknowledge S. Izvekov for providing the force-matching routines that were used in analysis shown in the inset of Figure 4, and F. Gygi for many useful discussions. This work was performed under the auspices of the U.S. Dept. of Energy at the University of California/Lawrence Livermore National Laboratory.

Competing interests statement The authors declare that they have no competing financial interests.

Correspondence and requests for materials should be addressed to S.A.B. (bonev1@llnl.gov).

UCRL-JRNL-216286

LAWRENCE
LIVERMORE
NATIONAL
LABORATORY

Carbon Under Extreme Conditions Phase Boundaries And Electronic Properties From First Principles Theory

A. A. Correa, S. Bonev, G. Galli

January 31, 2006

Proceedings of the National Academy of Science

Disclaimer

This document was prepared as an account of work sponsored by an agency of the United States Government. Neither the United States Government nor the University of California nor any of their employees, makes any warranty, express or implied, or assumes any legal liability or responsibility for the accuracy, completeness, or usefulness of any information, apparatus, product, or process disclosed, or represents that its use would not infringe privately owned rights. Reference herein to any specific commercial product, process, or service by trade name, trademark, manufacturer, or otherwise, does not necessarily constitute or imply its endorsement, recommendation, or favoring by the United States Government or the University of California. The views and opinions of authors expressed herein do not necessarily state or reflect those of the United States Government or the University of California, and shall not be used for advertising or product endorsement purposes.

Carbon under extreme conditions: phase boundaries and electronic properties from first-principles theory

Alfredo A. Correa
Department of Physics, University of California at Berkeley, Berkeley, California 94720, USA
Lawrence Livermore National Laboratory, Livermore, California 94550, USA

Stanimir A. Bonev
Department of Physics, Dalhousie University, Halifax, Nova Scotia B3H 3J5, Canada
Lawrence Livermore National Laboratory, Livermore, California 94550, USA

Giulia Galli
Lawrence Livermore National Laboratory, Livermore, California 94550, USA *
(Dated: December 4, 2005)

At high pressure and temperature, the phase diagram of elemental carbon is poorly known. We present predictions of diamond and BC8 melting lines and their phase boundary in the solid phase, as obtained from first principles calculations. Maxima are found in both melting lines, with a triple point located at ~ 850 GPa and ~ 7400 K. Our results show that hot, compressed diamond is a semiconductor which undergoes metalization upon melting. In contrast, in the stability range of BC8, an insulator to metal transition is likely to occur in the solid phase. Close to the diamond/ and BC8/liquid boundaries, molten carbon is a low-coordinated metal retaining some covalent character in its bonding up to extreme pressures. Our results provide constraints on the carbon equation of state, which is of critical importance for devising models of Neptune, Uranus and white dwarf stars, as well as of extra-solar carbon-rich planets.

Elemental carbon has been known since prehistory, and diamond is thought to have been first mined in India more than 2000 years ago, although recent archaeological discoveries point at the possible existence of utensils made of diamond in China, as early as 4000 BC[1]. Therefore, the properties of diamond and its practical and technological applications have been extensively investigated for many centuries. In the last few decades, following the seminal work of Bundy and coworkers in the 1950's and 60's[2], widespread attention has been devoted to studying diamond under pressure[3]. For example, the properties of diamond and, in general, of carbon under extreme pressure and temperature conditions are needed to devise models of outer planet interiors (e.g. Neptune and Uranus)[4, 5, 6], white dwarfs[7, 8] and extra-solar carbon planets[9].

Nevertheless, under extreme conditions the phase boundaries and melting properties of elemental carbon are poorly known, and its electronic properties are not well understood. Experimental data are scarce due to difficulties in reaching megabar pressures and thousands of Kelvin regimes in the laboratory. Theoretically, sophisticated and accurate models of chemical bonding transformations under pressure are needed in order to describe phase boundaries. In most cases, such models cannot be simply derived from fits to existing experimental data, and one needs to resort to first principles calculations, which may be very demanding from a computational standpoint.

It has long been known that diamond is the stable phase of carbon at pressures above several GPa[2]. Total energy calculations[10, 11] based on Density Functional Theory (DFT) predict a transition to another four-fold coordinated phase with the BC8 symmetry* at ~ 1100 GPa and 0 K, followed by a transition to a simple cubic phase at pressures above 3000 GPa. These transitions have not yet been investigated experimentally, as the maximum pressure reached so far in diamond anvil cell experiments on carbon is 140 GPa[14]. The only experimental information on diamond melting in the $\sim 10^2 - 10^3$ GPa range is from recent shock-wave experiments, where melting and a transition to a conducting fluid were observed [15]. However, these measurements were insufficient to locate phase boundaries and inconclusive as to whether diamond undergoes an insulator to metal transition before or after melting.

A number of experimental studies[16, 17] and *ab initio* simulations [18, 19, 20] have focused on the phase boundaries close to the graphite-diamond-liquid triple point (around 4000 K and 15 GPa). Unlike other solids with the diamond structure (e.g., Si, Ge), at these pressures the melting line of carbon has a positive slope[19]. However, at much higher pressure (several hundred GPa's), Martin and Grumbach[21] suggested that the slope becomes negative. This result was inferred from the comparison of the specific volumes of liquid and solid carbon, computed from *ab initio* molecular dynamics. Empirical potentials[22, 23, 24, 25] have also been employed to investigate melting of carbon with different degrees of success. In general, empirical potentials lack predictive power over large density variations and, more

*Present address: Department of Chemistry, University of California at Davis, Davis, CA 95616

* BC8 has been experimentally shown to be a metastable phase of silicon[12] and germanium[13] and therefore proposed as a possible high pressure phase of carbon.

specifically, important discrepancies between *ab initio* calculations and empirical potentials have been recently found, e.g. for the existence of a liquid/liquid phase transition at low pressure[20, 24, 26].

In this paper, we report on the properties of carbon in the pressure and temperature range of 15 to 2000 GPa and 0 to 10000 K, as obtained from first principles calculations based on DFT. We have investigated solid/liquid phase boundaries and analyzed structural and electronic transformations as pressure and temperature are increased. In particular, we have determined diamond and BC8 melting lines and predicted the location of the diamond/BC8/liquid triple point, inferred from the crossing of computed phase boundaries. Structural and electronic properties of diamond and BC8, and the solid/solid transition in this range of temperatures have also been investigated by a combination of different techniques.

Method. We carried out electronic structure calculations and first principles molecular dynamics (MD) using DFT in the generalized gradient-corrected approximation (GGA); we employed norm-conserving pseudopotentials to describe the interaction between core and valence electrons and we expanded single particle orbitals in plane waves[†]. Simulations were carried out within the adiabatic Born-Oppenheimer approximation, where the electronic ground state is computed self-consistently at each ionic step. The adiabatic approach is efficient for handling the small or null electronic band gap of the liquid phase of compressed carbon, and it allowed us to use ionic time steps up to 10 a.u.

We first computed the equation of state of diamond at zero temperature, in order to test the accuracy of our theoretical and numerical approach. The agreement with the available experimental data in the range $0-140$ GPa[14] is excellent. For example, the computed equilibrium volume only differs by 1% from the experimental value, and optical phonon frequencies agree with experiment within 3%[14]. This level of accuracy is already obtained with 64-atom supercells and a Γ-point sampling of the Brillouin zone, as evident from convergence tests performed with supercells containing up to 216 atoms and with unit cells with up to $12\times12\times12$ k-point meshes. Consistent with previous studies, we find that, at zero temperature, the transition pressure from diamond to BC8 is 1075 GPa. Other candidate structures previously proposed in the literature, such as R8[28], ST12[29] and hexagonal diamond[30], were also examined but were found to be unstable relative to BC8 in the pressure range studied here.[‡]

Calculations of diamond and BC8 melting lines were carried out by direct simulation of solid/liquid coexistence (i.e., by using a so-called two-phase simulation method). This approach has been recently shown to be applicable and efficient within the framework of *ab initio* MD simulations of comparable scale[31, 32, 33]. The two-phase method consists in choosing a given thermodynamic condition in (P,T) space, where liquid and solid systems are prepared and equilibrated. They are then put in contact and constant pressure-constant temperature simulations are carried out to determine which of the two phases is more stable at that given (P,T): as simulation progresses, the more stable phase eventually fills the entire volume available in the simulation. The melting line is located by repeating this process at different (P_n,T_n) points. Several complementing criteria, including diffusion coefficients, were used to determine whether melting or crystallization occurs. In addition, correlation functions, coordination numbers, and local order parameters[34] were computed throughout all simulations to monitor the time evolution of the solid/liquid interfaces.

In the simulations of diamond/liquid coexistence and BC8/liquid coexistence we used 128 and 256 atom cells respectively, with half of the atoms initially in a solid and the other half in a liquid state. For selected thermodynamic conditions, we also repeated calculations of diamond/liquid coexistence with 256 atom cell (i.e. doubled in the direction perpendicular to the solid-liquid interface), in order to assess errors introduced by finite size effects on the calculated melting lines. In addition, we compared two-phase simulations carried out with finite and with zero electronic temperature, for selected points in phase space; at pressures above 1000 GPa we assessed the error of the pseudopotenial approximation by repeating some of our simulations using a pseudopotential with a smaller cut off radius (decreased from 1.4 to 1.14 a.u., and consequently a higher plane wave cutoff, increased to 70 Ry). We used s, p non-local and d local potentials. In contrast to the low pressure regime where the bonding is dominated by s-p hybridization, at extreme pressures, an accurate description of the d channel is important because the coordination of the liquid becomes larger than four and configurations other than tetrahedral are present in the molten phase.

Finally, we determined the diamond/BC8 phase line using two independent approaches: (i) by combining results from two-phase simulations with equation of state calculations near the diamond/BC8/liquid triple point, and (ii) from calculations of the free energies of diamond and BC8, based on the quasi-harmonic approximation and including quantum ionic motion.

Phase boundaries. The computed melting lines of diamond and BC8 are shown in Fig. 1. The internal consistency of our simulations was verified by computing the slope of melting lines from the Clapeyron equation ($dP/dT_{\rm m} = \Delta H/T_{\rm m}\Delta V$), where the specific volume (ΔV) and enthalpy (ΔH) are obtained from one-phase simulations, while the melting temperature ($T_{\rm m}$) at which these quantities are computed is taken from the two-phase results (Fig. 1.)

A detailed error analysis shows that at high pressure (above 500 GPa) errors introduced by finite size effects and by neglecting the finite electronic temperature ($T_{\rm e}$) are of opposite sign. The melting temperature of diamond increases by about

---

[†] Periodic boundary conditions and a plane wave basis with a 50 Ry energy cutoff and Troullier-Martins pseudopotential[27] were used in this work. Our *ab initio* MD simulations were carried out with the Qbox code, written by F. Gygi. Static calculations of electronic properties and total energy convergence with k-points were obtained through the use of the ABINIT code (a common project of the Université Catholique de Louvain, Corning Incorporated, and other contributors.)

[‡] The discrepancy with previous reports on the stability of R8 stems from the numerical accuracy of the calculations that have appeared in the literature, which were not fully converged as a function of plane wave cutoff and k-point sampling.

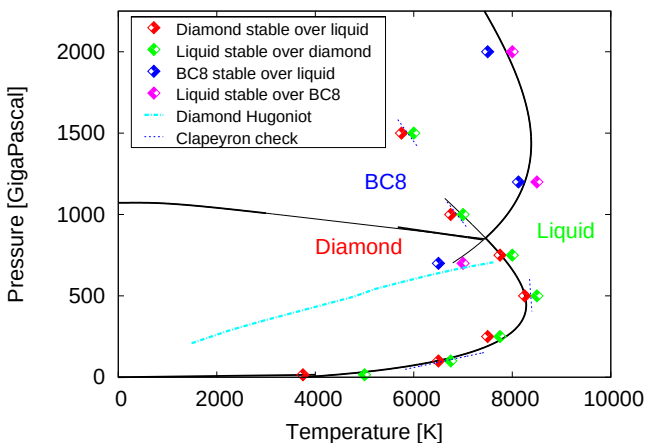

FIG. 1: Calculated phase diagram of carbon at high pressure, omitting the graphite stability region for clarity. Points indicate the final two-phase simulation data used to bracket the melting temperatures. The plotted melting lines are a fit to the melting points, using the three-parameter Kechin melting equation[35]. For a consistency check, the slopes of the melting curves (marked with short dotted segments) were computed independently from the Clapeyron equation[36]. The phase boundary between diamond and BC8 is calculated within the quasi-harmonic approximation at low temperature and from the three-phase Clapeyron identity Eq. 1 near the triple point. The triple point is located at $T = 7445$ K and $P = 850$ GPa; metastable extensions of melting lines of BC8 and diamond are calculated and presented for illustrative purposes. The diamond Hugoniot (dashed line) is shown for comparison with experimental results (see text.)

200 K in going from 128- to 256-atom simulation cells (at $P = 1000$ GPa), but it decreases by about 500 K when considering $T_e \sim 8000$ K in our calculation with 128-atom simulation cells (at 500-750 GPa and 8000 K). Introducing electronic temperature likely reduces the directional character of the interatomic forces in the liquid, thus increasing the number of effective degrees of freedom of the ions; in turn this results in an increase of the ionic entropy and hence a reduction of the free energy of the liquid relative to the that of the solid. On the other hand, the introduction of a electronic temperature has little or even a null effect on the insulating solid. In addition, we found a variation of the melting temperature of about 200 K at 1000 GPa on decreasing the pseudopotential cutoff radius; this effect diminishes rapidly at lower pressures.

While we estimate our numerical errors to be about $\pm 150/250$ K at fixed pressure, the error introduced by DFT is more difficult to quantify. We note that in cases where the electronic charge density tends to be more homogeneous in the liquid phase than in the solid, the GGA is expected to favor the former phase and thus to underestimate the meting temperature. This is the case, for example, for Al, Si, LiH and it is likely to be so for diamond and BC8 as well. Although quantitative estimates for carbon are difficult to make in the absence of experimental data and calculations beyond the GGA, it is worth noting that for Si, the melting temperature at ambient conditions is underestimated by about 10 %, and this error is expected to decrease as pressure is increased[32, 37].

The melting line of diamond obtained in our calculations is consistent with that reported by Grumbach and Martin[21], although the triple point found here is at a lower pressure than one might infer from the results of Ref. [21]. Our predicted diamond melting temperatures are also lower than those obtained in recent calculations with semi-empirical potentials[26], especially in the high pressure region. The reason for this discrepancy may come from the data set to which the empirical potentials have been fitted, which only contains low pressure, mostly tetrahedral, structures. We note that the gradual change in coordination number found here is the key for understanding the changes in the volume of the liquid relative to the solid as pressure is increased, and it is responsible for the existence of a maximum on the melting line, as we discuss below.

As apparent from Fig. 1, both diamond and BC8 melting lines have maxima slightly above 8000 K, at ~ 450 and ~ 1400 GPa, respectively. The physical origin of these maxima stems from the changes which covalent interactions undergo upon compression. A signature of these changes can already be found at low temperature. Fig. 2 shows the zero temperature phonon dispersion curves in diamond as a function of pressure. As reported in Ref.[38], acoustic branches of the phonon dispersion are rather flat near the Brillouin zone boundaries. In addition, the frequencies of the transverse acoustic branches near the L and X symmetry points have a maximum as a function of pressure. While their softening above ~ 250 GPa cannot destabilize the diamond structure at low temperature, it points at a loss of stability of the sp^3 hybridization as a function of pressure. Similar effects appear also in the the liquid phase at high temperature, where they are responsible for more dramatic changes in the liquid structure upon compression.

In order to analyze the structure of the molten phase, we have computed the pair correlation function and the coordination number of the liquid at different pressures (Fig. 3), close to the melting line. Unlike Si and Ge, we find that liquid carbon retains a partial covalent character in its bonding up to extreme pressures. We also find that the coordination of the fluid is lower than that reported in previous *ab initio* works[21]. The changes taking place in the liquid, which are responsible for the maxima in the melting lines, are illustrated in Fig. 3 where we report the number of differently coordinated sites as a function of P. The fraction of 4-fold coordinated atoms has a maximum near 400 GPa, while that of 5-fold coordinated atoms peaks between 1000 and 1500 GPa. These maxima correspond to the maxima on the melting line, displayed in Fig. 1.

The intersection of the diamond and BC8 melting lines yields the location of a solid/solid/liquid triple point at 7445 K and 850 GPa. The phase boundary between the two solid phases close to the triple point can be calculated from the Clapeyron equation with the use of the computed slopes of the melting lines and equilibrium volumes of the three phases:

$$\left(\frac{dP}{dT}\right)_{\mathrm{DB}} = \frac{\Delta S_{\mathrm{DB}}}{\Delta V_{\mathrm{DB}}} = \frac{\Delta V_{\mathrm{DL}}\left(\frac{dP}{dT}\right)_{\mathrm{DL}} - \Delta V_{\mathrm{BL}}\left(\frac{dP}{dT}\right)_{\mathrm{BL}}}{\Delta V_{\mathrm{DB}}} \quad (1)$$

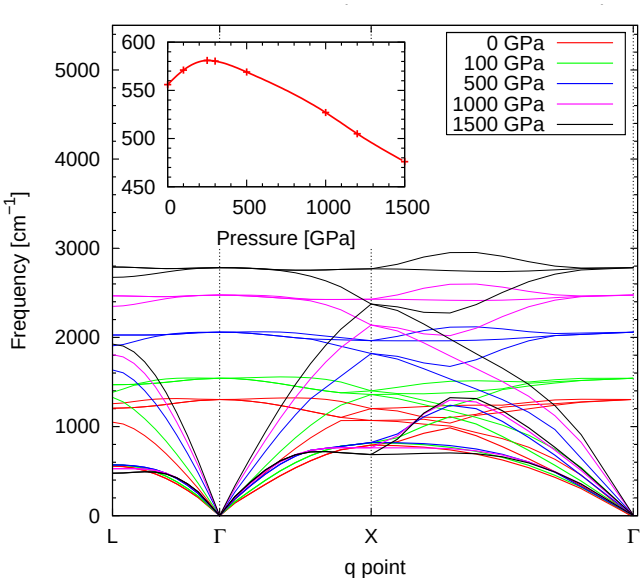

FIG. 2: Phonon dispersion curves of diamond calculated at different pressures; transverse acoustic (TA) branches are highlighted. Inset: Pressure dependence of TA phonon at the L point: note the maximum in phonon frequency at 250 GPa (see text.)

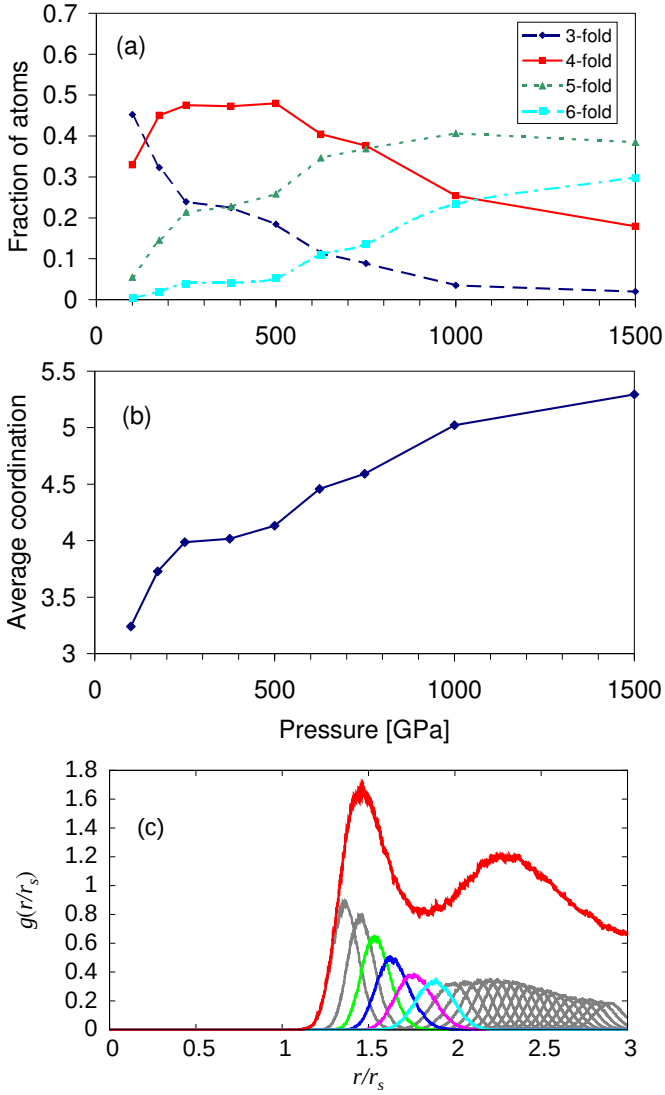

FIG. 3: (a) Fraction of 3, 4, 5 and 6-fold coordinated atoms as a function of pressure at $T = 9000$ K in liquid carbon. The coordination of each atom is computed by counting the number of its neighbors within a distance less than the first minimum of the pair correlation function. (b) Average coordination in the liquid phase as a function of pressure ($T = 9000$ K), obtained by integrating the normalized pair correlation function up to its first minimum. (c) Pair correlation function, together with histogram of distances of the first 24 neighbors, at $P = 1000$ GPa and $T = 9000$ K. At this pressure and temperature, the maximum of the histogram curve for the fifth neighbor is shown to be just inside the first peak of the pair correlation function.

Here subscripts D, B and L indicate diamond, BC8 and liquid phases, respectively, and all quantities are evaluated at the triple point. With this approach, difficulties associated with the explicit computation of free energies are avoided and the results do not rely on the harmonic approximation, which may not be valid at high temperature.

We find that the BC8/diamond phase boundary has a negative slope (Fig. 1) near the triple point. The difference between ours and that of Ref. [21] is not too surprising, as the phase stability presented in Ref. [21] came from estimates based on the Lindeman criterion. The stability of BC8 relative to diamond is apparently enhanced at high temperature, possibly as a result of additional degrees of freedom in bonding angle configurations (as geometrically described in Ref. [39].)

At low temperature, the diamond-BC8 boundary is evaluated by carrying out free energy calculations in the quasi-harmonic approximation. We have computed the full phonon dispersion relations for both the diamond and BC8 phases[40] and obtained the phonon energy and entropy by integration of the specific heat over temperature. The coexistence line between BC8 and diamond is then determined by matching the values of the Gibbs free energies –i.e., $G_{\rm D}(T_{\rm coex}, P_{\rm coex}) = G_{\rm B}(T_{\rm coex}, P_{\rm coex})$.– Our results, presented in Fig. 1, show a phase boundary that starts at 1075 GPa at zero temperature and has a negative pressure versus temperature slope at finite temperature. We note that zero point energy effects were taken into account and they reduce the diamond/BC8 transition pressure by 62 GPa at zero temperature, relative to a classical total energy calculation.

Finally, we note that by extrapolating the low temperature diamond/BC8 transition line, we obtain an accurate matching with the transition line near the triple point, as determined by Eq. 1 (Fig. 1.) The excellent agreement between the slopes of the phase boundaries obtained with three different methods: (i) free energy matching (ii) two-phase simulation for the location of the diamond/BC8/liquid triple point (iii) diamond/BC8 slope calculated with Eq. 1, is evidence for the accuracy and consistency of the computed phase boundaries.

Changes of electronic properties upon melting. Finally, we turn to the discussion of electronic properties of carbon under extreme conditions. It is well known that at zero temperature, the band gap of diamond increases with pressure, and this result is reproduced in our calculations. The GGA approx-

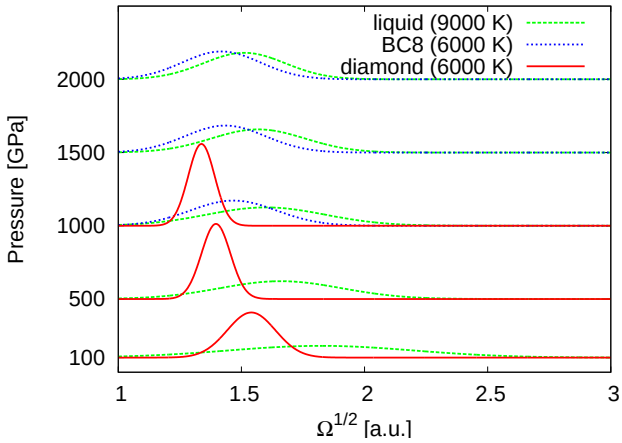

FIG. 4: Maximally localized Wannier function (MLWF) spreads for diamond ($T = 6000$ K), BC8 ($T = 6000$ K) and liquid ($T = 9000$ K) phases at selected pressures. While in insulating diamond the MLWF spread is significantly reduced with pressure (gap of diamond increases with pressure), the metallic liquid maintains larger spreads across a broad range of pressures. BC8, being a semiconductor with a small gap ($\sim$ 0.4 eV at $T \simeq 0$), is an intermediate case.

imation is known to underestimate the gap, compared both to experiment[41, 42] (5.45 eV) and calculations with many-body corrections (5.6 eV)[43]. In order to study whether diamond metalizes before melting, we have investigated the gap determined by the single particle energy difference between the highest occupied orbital and the lowest unocuppied orbital (HOMO-LUMO gap) of the solid as a function of P and T. Snapshots from 64-atom molecular dynamics were selected and electronic structure calculation of the gap and the electrical conductivity (using the Kubo formula[44]) were carried out using dense k-point meshes (up to $6 \times 6 \times 6$).

The calculated electronic gap of diamond decreases steadily with temperature at constant pressure (this was shown also to be a trend at ambient pressure and low temperature by experimental work[45]); however the zero temperature DFT-GGA gap (ranging from 4.4 eV at $P = 0$ to 6.9 eV at $P = 1100$ GPa) is so large that temperature effects are not sufficient to close the gap before melting occurs. For example at $P = 1000$ GPa, the gap reduces from 6.8 eV at $T = 0$ to 3.6 ± 0.5 eV at the melting temperature (6750 K). In our simulations the diamond DFT gap remained finite even at temperatures where the solid is likely to be superheated (i.e., metastable.) Frequency-dependent conductivity calculations confirm that the HOMO-LUMO gaps correspond to the optical gaps. The liquid, instead, shows a continuous density of states at the Fermi level and a finite conductivity at zero frequency. Thus, we conclude that diamond remains an insulator in the solid phase, and an insulator-to-metal transition occurs only upon melting. Figure 4 shows the spread of the *maximally localized Wannier functions* (MLWF)[46] as a function of pressure, at fixed temperatures. The marked difference between the spread found in diamond and the fluid attest to the qualitative difference between their electronic properties.

Our results are consistent with recent shock-wave experiments[15] where a transition was found to a conducting phase (revealed by a reflectance change) along the Hugoniot upon shock compression at around $600 - 700$ GPa. The diamond Hugoniot crosses our calculated melting line at $P = 720$ GPa (Fig. 1) and, as in the case of the experiment, we predict a transition from an insulating solid phase to a conducting liquid phase.

The gap of BC8 has a very different behavior than that of diamond; it is much smaller in the region where BC8 is stable (see the corresponding MLWF spreads in Fig. 4.) The DFT-GGA gap of BC8 is below 0.45 eV at $T = 0$ at the diamond/BC8 transition point and it slightly decreases with pressure. This small gap makes it difficult to assert a prediction on the metallic nature of this phase at finite temperature. If disorder reduces the gap at the same rate as in the case of the diamond phase, then BC8 is likely to become metallic in the solid phase at relatively low temperature, before melting.

In conclusion, we have reported a first principles computational study of the phase diagram of carbon and we have determined solid/liquid and solid/solid phase boundaries up to $\sim$ 2000 GPa and $\sim$ 10000 K. Our results provide a consistent description of elemental carbon in a broad range of temperature and pressures and a description of its electronic properties is given within the same framework. The diamond/BC8/liquid triple point is found to be at lower pressure than previously thought; in particular this point is close to recent estimates[47, 48, 49] of the Neptune and Uranus core conditions. While some old estimates locate the core conditions in the diamond stability region determined here (7000 K, 600 GPa)[47], newer estimates point at conditions were the liquid is stable instead (8000 K, 800 GPa)[48, 49]. Therefore, our data call for a partial revision of current planetary models, especially in the planetary core regions. Overall this work provides constraints to the carbon equation of states and it may help to interpret future experimental work.

This work was performed under the auspices of the U.S. Department of Energy at the University of California/Lawrence Livermore National Laboratory under Contract No. W-7405-Eng-48. S.B. acknowledges support from NSERC of Canada. We thank Francois Gygi, Tadashi Ogitsu, Eric Schwegler, Xiaofei Wang and Roberto Car for many useful discussions; we also thank Roger Falcone for his constant help and support and for a critical reading of the manuscript.

[1] Lu, P. J, Yao, N, So, J. F, Harlow, G. E, Lu, J. F, Wang, G. F, & Chaikin, P. M. (2005) *Archaeometry* **47**, 1.
[2] Bundy, F, Hall, T, Strong, H. M, & Wentorf, R. H. (1955) *Nature* **176**, 51.
[3] Bundy, F. P, Bassett, W. A, Weathers, M. S, Hemley, R. J, Mao, H. K, & Goncharov, A. F. (1996) *Carbon* **34**, 141.

[4] Ross, M. (1981) *Nature* **292**, 435.
[5] Hubbard, W. B. (1981) *Science* **214**, 145.
[6] Benedetti, L. R, Nguyen, J. H, Caldwell, W. A, Liu, H, Kruger, M, & Jeanloz, R. (1999) *Science* **286**, 100–102.
[7] Segretain, L, Chabrier, G, Hernanz, M, Garcia-Berro, E, Isern, J, & Mochkovitch, R. (1994) *Astroph. J.* **434**, 641–651.
[8] Metcalfe, T. S, Montgomery, M. H, & Kannan, A. (2004) *Astroph. J.* **605**, L133–L136.
[9] Kuchner, M. J & Seager, S. (2005) *Astroph. J. (in press)*.
[10] Yin, M. T & Cohen, M. L. (1984) *Phys. Rev. Lett.* **50**, 2006.
[11] Yin, M. T. (1984) *Phys. Rev. B* **30**, 1773.
[12] Hu, J. Z, Merkle, L. D, Menoni, C. S, & Spain, I. L. (1994) *Phys. Rev. B* **34**, 4679.
[13] Nelmes, R. J, McMahon, M. I, Wright, N. G, Allan, D. R, & Loveday, J. S. (1993) *Phys. Rev. B* **48**, 9883.
[14] Occelli, F, Loubeyre, P, & Letoullec, R. (2003) *Nature Mater.* **2**, 154.
[15] Bradley, D. K, Eggert, J. H, Hicks, D. G, Celliers, P. M, Moon, S. J, Cauble, R. C, & Collins, G. W. (2004) *Phys. Rev. Lett.* **93**, 195506.
[16] Weathers, M. S & Bassett, W. A. (1987) *Phys. Chem. Miner.* **15**, 105.
[17] Togaya, M. (1990) *High Press. Res.* **4**, 342.
[18] Galli, G, Martin, R. M, Car, R, & Parrinello, M. (1989) *Phys. Rev. Lett.* **63**, 988.
[19] Galli, G, Martin, R. M, Car, R, & Parrinello, M. (1990) *Science* **250**, 1547–1549.
[20] Wu, C. J, Glosli, J. N, Galli, G, & Ree, F. H. (2002) *Phys. Rev. Lett.* **89**, 135701.
[21] Grumbach, M. P & Martin, R. (1996) *Phys. Rev. B* **54**, 15730.
[22] Brenner, D. W. (1990) *Phys. Rev. B* **42**, 9458–9471.
[23] van Thiel, M & Ree, F. H. (1992) *High Press. Res.* **10**, 607.
[24] Glosli, J. N & Ree, F. H. (1999) *Phys. Rev. Lett.* **82**, 4659.
[25] Fried, L. E & Howard, W. M. (2000) *Phys. Rev. B* **61**, 8734.
[26] Ghiringhelli, L. M, Los, J. H, Meijer, E. J, Fasolino, A, & Frenkel, D. (2005) *Phys. Rev. Lett.* **94**, 145701.
[27] Troullier, N & Martins, J. L. (1991) *Phys. Rev. B* **43**, 1993.
[28] Clark, S. J, Ackland, G. J, & Crain, J. (1995) *Phys. Rev. B* **52**, 15035.
[29] Biswas, R, Martin, R. M, Needs, R. J, & Nielsen, O. H. (1987) *Phys. Rev. B* **35**, 9559.
[30] Bundy, F. P & Kasper, J. S. (1967) *J. Chem. Phys.* **46**, 3437–3446.
[31] Ogitsu, T, Schwegler, E, Gygi, F, & Galli, G. (2003) *Phys. Rev. Lett.* **91**, 175502.
[32] Alfe, D. (2003) *Phys. Rev. B* **68**, 064423.
[33] Bonev, S. A, Schwegler, E, Ogitsu, T, & Galli, G. (2004) *Nature* **431**, 669.
[34] Steinhardt, P. J, Nelson, D. R, & Ronchetti, M. (1983) *Phys. Rev. B* **28**, 784.
[35] Kechin, V. V. (2002) *Phys. Rev. B* **65**, 052102.
[36] Zemansky, M. W. (1968) *Heat and Thermodynamics, 5th ed.* (McGraw-Hill, New York).
[37] Sugino, O & Car, R. (1995) *Phys. Rev. Lett.* **74**, 1823.
[38] Xie, J, Chen, S. P, Tse, J. S, de Gironcoli, S, & Baroni, S. (1999) *Phys. Rev. B* **60**, 9444–9449.
[39] Crain, J, Clark, S. J, Ackland, G. J, Payne, M. C, Milman, V, Hatton, P. D, & Reid, B. J. (1994) *Phys. Rev. B* **49**, 5329.
[40] Tsuchiya, J, Tsuchiya, T, & Wentzcovitch, R. M. (2005) *J. Geophys. Res.* **110**, B02204.
[41] Schulz, M & Weiss, H. (1982) *Landolt-Börnstein Tables, Numerical Data and Functional Relationships in Science and Technology* ed. Madelung, O. (Springer, Berlin) Vol. New Series, 17a.
[42] Dean, P. J, Lightowlers, E. C, & Wight, D. R. (1965) *Phys. Rev.* **140**, A352.
[43] Surh, M. P, Louie, S. G, & Cohen, M. (1992) *Phys. Rev. B* **45**, 8239.
[44] Kubo, R. (1957) *J. Phys. Soc. Jap.* **12**, 570–586.
[45] Papadopoulos, A. D & Anastassakis, E. (1990) *Phys. Rev. B* **43**, 9916.
[46] Souza, I, Martin, R. M, Marzari, N, Zhao, X, & Vanderbilt, D. (2000) *Phys. Rev. B* **62**, 15505.
[47] Stevenson, D. J. (1982) *Annu. Rev. Earth Planet. Sci.* **10**, 257–295.
[48] Guillot, T. (1999) *Science* **286**, 72–77.
[49] Guillot, T. (2005) *Annu. Rev. Earth Planet. Sci.* **33**, 493–530.